

Planet formation regulated by galactic-scale interstellar turbulence

Andrew J. Winter¹, Myriam Benisty^{1,2}, Sean M. Andrews³

ABSTRACT

Planets form from protoplanetary discs of dust and gas that surround stars younger than a few million years.¹ The properties of these discs dictate how planets grow, determining the nature, architecture and composition of the observed exoplanet population. The nature of (turbulent) angular momentum transport through the disc in particular is critical for planet growth² and migration.^{3,4} While the dominant physical processes in disc evolution remain unknown, theoretical studies widely assume an isolated star-disc system. Here we challenge this conventional assumption by showing that, far from being isolated systems, discs in typical star forming environments are constantly replenished by capturing new material from the interstellar medium (ISM). We show that this in-fall alone explains observed disc masses, outer radii and stellar accretion rates as a function of time and stellar mass. ISM capture is also capable of driving disc turbulence corresponding to viscosity in the range $\alpha_{SS} \sim 10^{-5} - 10^{-1}$, as observationally inferred.⁵⁻⁷ We find that 20–70 percent of discs are composed of material captured in the most recent half of their life-time, implying their properties are not direct probes of internal disc physics. Our results suggest that planet formation is driven by the

¹Université Côte d’Azur, Observatoire de la Côte d’Azur, CNRS, Laboratoire Lagrange, 06300 Nice, France

²Université Grenoble Alpes, CNRS, IPAG, 38000 Grenoble, France

³Center for Astrophysics — Harvard & Smithsonian, 60 Garden Street, Cambridge, MA 02138, USA

turbulent cascade of energy from galactic-scales down to the protoplanetary disc and that recent evidence of in-fall from the ISM onto mature protoplanetary discs⁸⁻¹⁰ are part of an important, general process. This represents a far-reaching shift in our understanding of every stage of planet formation, from dust aggregation to the migration of giant planets through the disc.

MAIN

Conventional models for planet formation assume that a protoplanetary disc forms during protostellar collapse, and then planets grow from material in the isolated star-disc system. This picture is now being challenged on a variety of fronts.^{11,12} Here we particularly explore the implications of recent *Atacama Large Millimeter/submillimeter Array* (ALMA) observations in molecular line emission¹³ and in infrared scattered light^{14,15} that are frequently revealing extended structures associated with protoplanetary discs, on spatial scales several times the disc outer radius. In-fall has been suggested as a possible origin for these structures,¹⁶⁻¹⁸ which are highly complex, including large scale spirals and streamers around T Tauri¹⁹ and Herbig AeBe²⁰ stars, often associated with reflection nebulosity,²¹ accretion outbursts²²⁻²⁴ and misaligned inner discs.²⁵ Evidence that is suggestive of in-fall events has been found not only during the earliest stages of disc evolution, when the star is still embedded in its natal environment,²⁶⁻²⁸ but also around stars such as AB Aur,^{8,29,30} DR Tau³¹ and SU Aur,²⁵ which are all mature star-disc systems of age $\sim 1-3$ Myr. A recent estimate from a sample size of 43 disc-hosting stars suggests approximately 16 percent are interacting with the ambient ISM.³² This material should fall onto the disc on a time-scale much shorter than

the disc lifetime,^{16,17} suggesting that either these events occur much more frequently than observed or the external structure is replenished by the ISM for a prolonged period. In-falling gas may be the consequence of Bondi-Hoyle-Lyttleton (BHL) accretion, where low velocity gas is captured due to the gravitational potential of the star.^{33,34} Theoretically, the rate of capture of material from the interstellar medium (ISM) via BHL accretion can be substantial while stars remain bound to a dense gas reservoir, and has been proposed to explain observed stellar accretion rates.^{35–37} However, assessing the importance of this process for the observed population of protoplanetary discs throughout their lifetime requires quantifying the temporal evolution of the turbulent ISM surrounding forming stars.

In this work, we statistically quantify the time evolution of the BHL accretion rate. We summarise the approach here and refer to the Methods for details. First, we apply an excursion set formalism^{38,39} to model fluctuations in the gas density and velocity in the solar neighbourhood. We use this to draw a representative sample of gravitationally unstable star forming regions that are common within ~ 200 pc of the sun (Extended Data Figure 1). We compute the evolution of the radius, density and star formation rate in these regions as they undergo free-fall collapse.⁴⁰ Star formation continues until the fraction of gas converted into stars is $\epsilon = 0.5$,⁴¹ at which time the bound gas is dispersed. Having computed the evolution of a representative sample of star forming regions, we draw formation times for a representative sample of 500 stars from these regions, weighted by the instantaneous star formation rate. We also draw individual star masses from a log-uniform distribution between $10^{-2} M_{\odot}$ and $3M_{\odot}$. Each star evolves within the potential of the collapsing star forming region from the time of formation until the dispersal of the region,

at which point the density and velocity structure local to the star-disc system is determined by the evolution of the unbound ISM. Density and velocity fluctuations in the galactic ISM evolve at different scales according to a generalised Fokker-Planck equation, resulting in drift-diffusion behaviour. We model this via a random-walk,³⁹ and can therefore compute the BHL accretion rate, being defined at the scale which maximises the rate of capture of material onto the star-disc system. In this way, we construct accretion histories for all of our stars.

We illustrate the outcome of these calculations in Figure 1, for a subset of six stars in our sample. The phase in which the star remains within the bound gaseous reservoir typically persists for ~ 1 Myr. During this phase, the relative velocity of the gas is low, $\Delta v_{\text{gas}} \lesssim 1 \text{ km s}^{-1}$ (Figure 1, top), in line with previous estimates.³⁷ Evidently, since the gas reservoir is gravitationally unstable, the local density ρ_{gas} (Figure 1, middle) is also large compared to the median density at the galactic mid-plane, which is $\rho_{\text{mid}} \sim 10^{-24} \text{ g cm}^{-3}$. This results in an early phase of enhanced BHL accretion at a median rate $\dot{M}_{\text{BHL},1/2} \sim 10^{-8} M_{\odot} \text{ yr}^{-1}$ (Figure 1, bottom). This median rate then quickly drops to $\dot{M}_{\text{BHL},1/2} \sim 10^{-10} - 10^{-11} M_{\odot} \text{ yr}^{-1}$ in the age range 1–3 Myr for a solar mass star. This is considerably lower than the typical rate of accretion onto the central star, $\dot{M}_{\text{acc}} \sim 10^{-8} - 10^{-9} M_{\odot} \text{ yr}^{-1}$.⁴² One might therefore assume that BHL accretion no longer plays an important role for disc evolution. However, in a turbulent medium, vorticity of the in-falling material means that accretion is mediated via a (protoplanetary) disc.^{17,43} In this case, the change in accretion rate can be averaged over the time-scale τ_{acc} at which angular momentum is transported within the disc. Empirically, this time-scale can be a considerable fraction of the disc lifetime.⁴⁴ In this case the median underestimates the true contribution of BHL accretion rate onto the disc to

the accretion rate onto the star. By contrast, the mean accretion rate when averaged over all stars in our model is $\langle \dot{M}_{\text{BHL}} \rangle \sim 10^{-8} - 10^{-9} M_{\odot} \text{ yr}^{-1}$ at 1 – 3 Myr, as shown as the dashed red line in Figure 1. However, the mean *overestimates* the typical BHL accretion rate contribution for individual discs, since it is dominated by a small number of rapid accretors. Interpreting the contribution from BHL accretion to the stellar accretion rate for typical star-disc systems is therefore not a simple task. Compounding this problem further, discs that survive to comprise the observed sample may also preferentially be those which have been replenished by the ISM. Interpreting the role of BHL accretion for disc evolution therefore requires further calculation.

To quantify the degree to which BHL accretion from the ISM sculpts observed protoplanetary disc properties, we perform a simple numerical experiment. For now, we remain agnostic to the mechanism by which accretion from the disc onto the star proceeds, parameterising the process by a single parameter $\tau_{\text{acc}} = M_{\text{disc}}/\dot{M}_{\text{acc}}$, where M_{disc} is the instantaneous disc mass. Then the rate of change of the disc mass as a function of time t is simply

$$\dot{M}_{\text{disc}}(t) = \dot{M}_{\text{BHL}}(t) - \frac{M_{\text{disc}}(t)}{\tau_{\text{acc}}}.$$

We assume that the initial disc mass is negligible, adopting $M_{\text{disc}}(t = 0) = 0$ (see Methods). We then make a parametric choice, anchoring τ_{acc} to observational constraints.⁴⁴ We draw a fixed τ_{acc} for each star, adopting a log-uniform distribution with ± 1 dex around $\log \tau_{\text{acc}}/1 \text{ Myr} = -0.5$. As a dispersal criterion, when $M_{\text{disc}} < 3 \times 10^{-5} M_{\odot}$ then we assume the star would be considered disc-less in observations. Our results are not dependent on this choice within a sensible range, and we are motivated by the fact that few discs are detected below this threshold. This threshold also results in a fraction of surviving discs in agreement with observational constraints (Extended

Data Figure 2). We further find that our calculations exhibit excellent agreement with the observed distributions of disc masses, stellar accretion rates, outer disc radii and constraints on turbulent velocities, as discussed below.

We show the disc properties in our model as a function of the stellar mass and age in Figure 2, comparing to observed discs in local star forming regions across a range of different ages. In order of increasing estimated age,⁴² these regions are ρ Ophiuchus, Taurus, Lupus, Chameleon I and Upper Scorpius (with the caveat that age estimates are uncertain and ages in Chameleon I, Taurus and Lupus overlap – see Methods). For nearly all these comparisons, we find remarkable agreement with the observed disc masses (Figure 2, top) and stellar accretion rates (Figure 2, middle) as a function of stellar host mass m_* and age. Both are typically limited by an upper ‘envelope’ that is a super-linear function of stellar mass, approximately $\propto m_*^2$, with a broad distribution below this upper limit for any given m_* . For older stars ($\gtrsim 1\text{--}2$ Myr), the masses and accretion rates decrease as discs are no longer rapidly replenished by BHL accretion. Observed accretion rates for Taurus and Upper Scorpius deviate somewhat from our model outcome, and these moderate differences must originate from some variation in τ_{acc} that we do not account for, since we choose to fix the τ_{acc} distribution. There may be several reasons for such variation (see Methods), and the overall agreement of our simple model with observations is striking. Interestingly, the discs in our model typically take a few 10^5 years to grow to a maximal mass (Extended Data Figure 3), which may explain the finding that the observationally inferred disc mass is not a monotonic function of age for very young star forming regions.^{45–47}

We can also attempt a comparison with the disc outer radii in our model and from observations. While we do not directly compute the disc radius R_{disc} in our model, we do track the radius from which material accretes onto the disc R_{acc} (see Methods). We generally expect $R_{\text{acc}} \gtrsim R_{\text{disc}}$, since the resultant disc radius depends on the vorticity of the in-falling material during the BHL accretion process.⁴³ However, it is reasonable to expect that $R_{\text{disc}} \propto R_{\text{acc}} \propto m_*$, assuming that the vorticity does not depend on m_* (or R_{acc}). While there are fewer measurements of gaseous disc outer radii in local star forming regions, in the bottom row of Figure 2 we compare our model to the empirically-inferred relationship for the outer gas disc radius as inferred from CO molecular line measurements: $R_{\text{CO}} = 250 (m_*/1 M_\odot)^{0.9}$ au,⁴⁸ typically a factor $\sim 2-3$ larger than the dust component, although with considerable scatter and some examples of much more extended CO radii.⁴⁹ We again find a remarkable similarity between our model results and the observed disc properties, with a tail of large $R_{\text{acc}} > R_{\text{CO}}$.

The striking agreement between the model results and the observational disc properties strongly supports the conclusion that the outer gaseous disc radii, total disc masses and stellar accretion rates are largely set by accretion from the ISM. This finding is particularly compelling given the simplicity of the model, relying only on established physical processes, without requiring fine tuning of free parameters. However, what is less clear is whether these properties are set by the initial phase of rapid accretion, or whether disc material is constantly replenished throughout the disc lifetime. To explore this, we define $f_{\text{M},1/2}$, which is the fraction of the current disc mass that was accreted from the ISM within the most recent half of the disc life-time (see Methods). This fraction is shown as a function of time for our 500 discs in Figure 3. We find that the distribution

of $f_{M,1/2}$ varies with time, with a greater fraction of discs being composed of recently accreted material early during their evolution. The fraction of discs that are not composed of any recently accreted material increases from approximately 20 percent at 1 Myr, to 50 percent for discs older than 3 Myr. This decrease is instigated by the drop in typical accretion rates at around 1 Myr (Figure 1), after which the majority of stars no longer inhabit the collapsing molecular cloud in which they were born. The fraction of discs that are *mostly* composed of recently accreted material ($f_{M,1/2} > 0.5$) remains approximately in the range 20 – 70 percent throughout the disc life-time. These estimates are conservative, since aside from stellar accretion we have not considered any internal processes, such as planet formation, that deplete disc material. We conclude that observed disc populations are constantly being replenished by the surrounding ISM, and that their properties therefore may not be direct probes of internal disc physics.

We have so far assumed that accretion onto the host star from the disc is driven by some, undefined internal angular momentum transport mechanism. However, we also expect some turbulence to be sustained due to the continuous in-fall of material. Material falls onto the disc at approximately the free-fall velocity, and then shocks as it hits the disc surface.⁵⁰ Some fraction ϵ_t of the energy deposited into the disc is kinetic, and the resultant turbulence may be sufficient to drive the turbulent velocity $v_{t,disc}$ empirically inferred for protoplanetary discs. We explore this possibility by computing the rate at which the turbulent energy evolves for our disc sample (see Methods). Turbulent energy decays rapidly within the disc, so BHL accretion onto the disc must be sustained. We can parameterise the strength of turbulence in terms of a Shakura-Sunyaev constant α_{SS} ,⁵¹ where $\alpha_{SS} \sim v_{t,disc}^2 / c_s^2$,⁵² for sound speed $c_s = 0.2 \text{ km s}^{-1}$.

Assuming efficiency $\epsilon_t = 1$, we show the resulting evolution of the $v_{t,\text{disc}}$ and α_{SS} distribution in Figure 4. At early times $\lesssim 1$ Myr, our calculation would suggest that the turbulent velocity can actually exceed c_s . Physically, this would produce shocks in addition to the initial shock from the free-fall onto the disc, and the resultant shock-heating would presumably substantially reduce ϵ_t . However, since the turbulent decay time-scale is short ($\sim 10^4$ years), $v_{t,\text{disc}}$ remains in an almost instantaneously determined balance between in-fall and turbulent decay. Therefore any deviation from $v_{t,\text{disc}}/c_s$ for the early disc in our model do not influence the subsequent distribution. We can therefore compare the turbulent velocity distribution to observational constraints at any time without worrying about a complex dependence on a time-varying ϵ_t . We note also the weak dependence of $v_{t,\text{disc}}$ on ϵ_t : $v_{t,\text{disc}} \propto \epsilon_t^{1/3}$, or $\alpha_{\text{SS}} \propto \epsilon_t^{2/3}$.

Observational constraints for the turbulent velocity in discs have yielded upper limits $v_{t,\text{disc}}/c_s \lesssim 0.05$ for older discs (age $\sim 5 - 10$ Myr) TW Hya,^{53,54} HD163296^{55,56}, MWC 480^{6,57} and V4046 Sgr,^{6,58} and high turbulence for the younger discs around DM Tau⁶ ($\sim 1-5$ Myr^{57,59}) and IM Lup⁶⁰ (~ 1 Myr⁶¹) with $v_{t,\text{disc}}/c_s \sim 0.25 - 0.33$ and $v_{t,\text{disc}}/c_s \sim 0.4 - 0.6$ respectively, corresponding to an high $\alpha \sim 0.1$. One of the most stringent constraints on turbulence in the mid-plane of a disc has been inferred from the vertical scale of dust in edge-on discs. One example is Oph163131, for which the extremely well-settled dust suggests a very low $\alpha_{\text{SS}} \sim 10^{-5}$.⁶² Consistent with the constraints on the turbulent velocity from line broadening, young discs have been shown to exhibit much less vertical settling of mm-sized dust grains.^{63,64} The distribution of α_{SS} that we obtain from our model imply that both discs with $\alpha_{\text{SS}} \sim 0.1$ (similar to DM Tau) and at the other extreme $\alpha_{\text{SS}} \sim 10^{-5}$ (similar to Oph163131) are possible if ϵ_t is just somewhat below unity. Our model

is also broadly consistent with the hint that older discs have lower levels of turbulence. We conclude that accretion from the ISM is capable of driving protoplanetary disc turbulence at the levels inferred for individual discs, providing $\epsilon_t \sim 0.1-1$.

A related question is whether the turbulence injected from the ISM is sufficient to drive observed accretion rates. To avoid adding prohibitive complexity to our model (see discussion in Methods), in this work we fix the accretion time-scale τ_{acc} (or turbulence) for each star-disc system, such that it is independent of the environment. However, we can estimate whether the capture of ISM material could feasibly drive turbulence at the same level that we assume in our distribution of τ_{acc} . To do so, we first rewrite⁶⁵

$$\tau_{\text{acc}} = \frac{M_{\text{disc}}}{\dot{M}_{\text{acc}}} = \frac{2R_1^2\Omega_1}{3\alpha_{\text{SS}}c_s^2} = 0.37 \left(\frac{\alpha_{\text{SS}}}{0.1}\right)^{-1} \left(\frac{R_1}{250 \text{ au}}\right)^{1/2} \left(\frac{m_*}{1 M_\odot}\right)^{1/2} \left(\frac{c_s}{0.2 \text{ km s}^{-1}}\right) \text{ Myr}, \quad (1)$$

for the stars with mass m_* with disc of scale radius R_1 , at which the Keplerian frequency is Ω_1 . Equation 1 applies for discs for which accretion from the disc onto the star is driven by turbulent viscosity, while the environmental dependence would enter via α_{SS} if turbulence were driven by ISM accretion. We generally expect R_1 to be smaller than the outer radius R_{CO} by a factor few, so we can estimate $R_1 = f_{\text{R}}R_{\text{CO}} \approx f_{\text{R}}250 (m_*/1 M_\odot)$ au to yield

$$\tau_{\text{acc}} \approx 0.2 \left(\frac{\alpha_{\text{SS}}}{0.1}\right)^{-1} \left(\frac{f_{\text{R}}}{0.3}\right)^{1/2} \left(\frac{m_*}{1 M_\odot}\right) \left(\frac{c_s}{0.2 \text{ km s}^{-1}}\right) \text{ Myr}. \quad (2)$$

For surviving discs, the median τ_{acc} in our model evolves from ~ 0.3 Myr to ~ 2 Myr over the course of ~ 9 Myr, as discs with short τ_{acc} are preferentially dispersed (Extended Data Figure 4). The median stellar mass in our model is $m_* \approx 0.2 M_\odot$, and therefore the early median accretion time-scale requires $\alpha_{\text{SS}} \sim 10^{-2}$, reducing to $\alpha_{\text{SS}} \sim 10^{-3}$ at later times. As shown in Figure 4,

this median α_{SS} is consistent with what we infer for the ISM driven turbulence from our model. This range of typical α_{SS} is also broadly consistent with observational constraints for stellar accretion rates.⁷ Within the BHL accretion scenario, we also expect some enhancement of the stellar accretion rate due to capture of material with low angular momentum, or angular momentum misaligned with the existing disc.⁶⁶ Overall, we conclude that capture of the ISM is a plausible driver of observed stellar accretion. However, we emphasise that this depends on the unknown ϵ_t , and our finding certainly does not preclude magnetically driven disc winds also contributing to angular momentum transport,⁶⁷ particularly in discs with low levels of turbulence.

In summary, we have shown accretion of the ISM is an important process in driving protoplanetary disc evolution. In particular, our three most important conclusions are:

1. Disc masses, radii and stellar accretion rates as a function of stellar mass and age can result directly from Bondi-Hoyle-Lyttleton accretion.
2. Material in the disc is constantly replenished over its lifetime. We estimate that 20–70 percent of discs are mostly composed of material captured in the most recent half of their lifetime. This estimate is conservative, ignoring processes apart from stellar accretion that might erode the existing disc, such as planet formation or winds.
3. The energy influx due to in-falling material onto the disc is sufficient to drive empirically inferred protoplanetary disc turbulence. We expect a broad distribution for α_{SS} , with typical value $\alpha_{\text{SS}} \sim 10^{-3}$, while some discs with much higher $\alpha_{\text{SS}} \sim 0.1$ (as for DM Tau) and lower $\alpha_{\text{SS}} \sim 10^{-5}$ (as for Oph163131) are expected.

If the ISM drives disc evolution, this represents a considerable change of direction for protoplanetary disc theory, which has largely focused on processes operating on an isolated star-disc system. Consequences of this new picture of disc evolution are fundamental and wide-reaching, relating to every stage of planet formation. The inextricable link between planet formation and the ISM underscores a great urgency for future observational and theoretical studies aiming to quantify how gas in-fall during formation influences protoplanetary disc structures, angular momentum transport and the observed exoplanet population.

Acknowledgements: We thank Cathie Clarke for useful discussion. AJW has received funding from the European Union's Horizon 2020 research and innovation programme under the Marie Skłodowska-Curie grant agreement No 101104656. This project has received funding from the European Research Council (ERC) under the European Union's Horizon 2020 research and innovation programme (PROTOPLANETS, grant agreement No. 101002188).

Competing interests: The authors declare no competing interests.

Materials & Correspondence: Requests for materials or correspondence should be addressed to A.J.W., currently at andrew.winter@oca.eu.

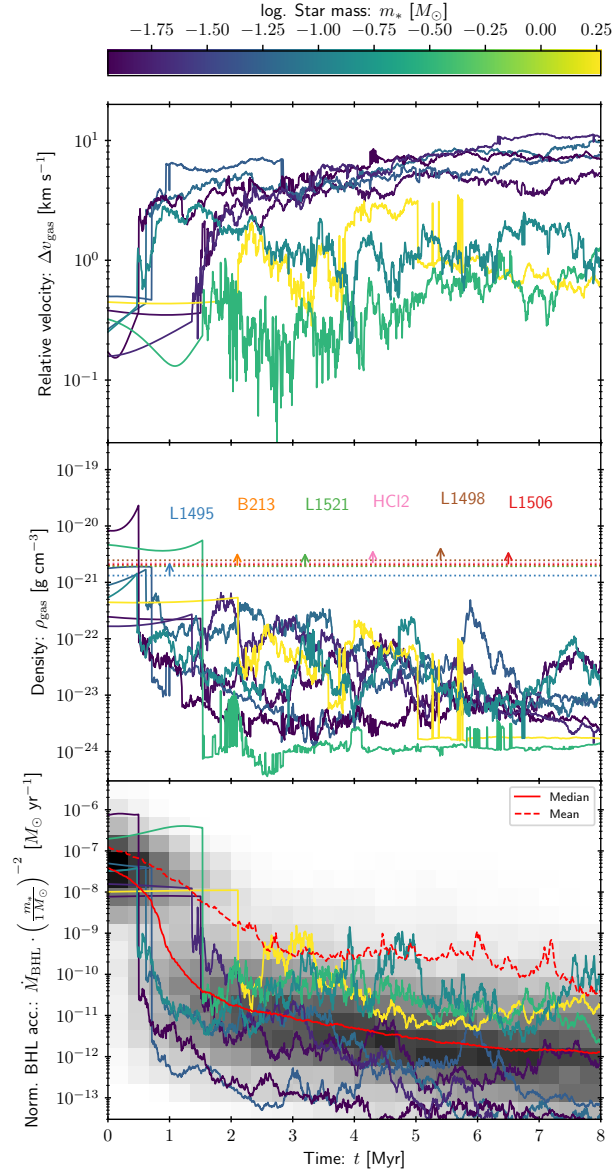


Figure 1: **Local velocity, density and normalised Bondi-Hoyle-Lyttleton accretion rates.** The relative velocity (top) and density (middle) of the local gas, for a subset of six stars in our sample of 500 trajectories. The BHL accretion rate (bottom) is normalised to be independent of mass m_* , by which lines are coloured. The gas density and velocity are shown at the accretion scale (see Methods). In the middle panel, the horizontal dotted lines are the mean gas density for some high density regions in Taurus (see Methods).⁶⁸ In the bottom panel, the red solid (dashed) line follows the median (mean) normalised BHL accretion rate for the entire sample, and a normalised two-dimensional histogram.

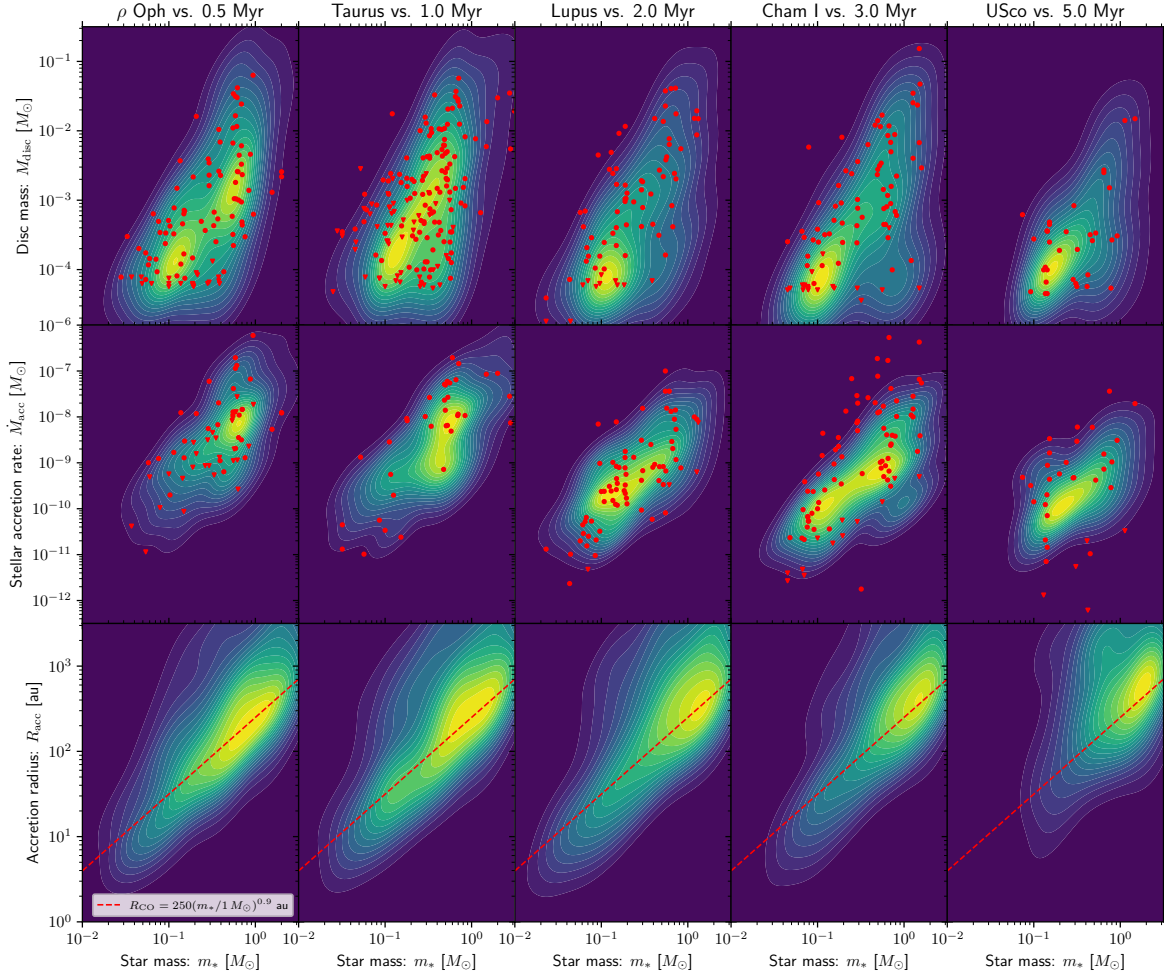


Figure 2: **Disc properties resulting from ISM accretion compared to observations.** Linear kernel density estimates (KDEs) for the disc mass (top), stellar accretion rate (middle) and accretion radii (bottom) versus stellar mass in our model compared to observations (red points, red dashed lines) in local star forming regions. We show results at times 0.5, 1, 2 and 3 and 5 Myr. The red points represent the distribution of $100\times$ dust disc masses (top), stellar accretion rate (middle) in ρ Ophiuchus, Taurus, Lupus, Chameleon I and Upper Scorpius (left to right).⁴² When constructing the KDEs, model points are weighted to yield the same distribution along the stellar mass axis as in the observational samples, except in the bottom row. For comparison with the accretion radii, we show the empirically inferred relationship between CO outer disc radii as a red dashed line in the bottom panels.⁴⁸

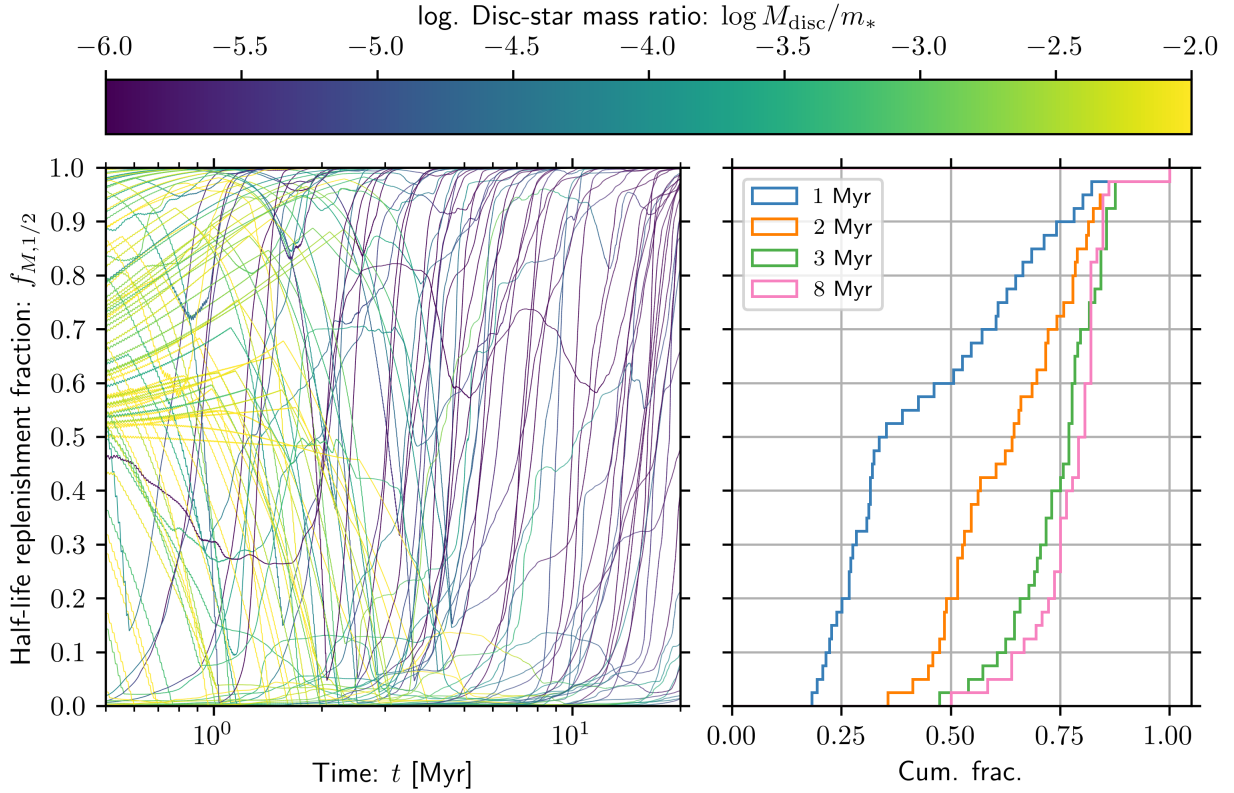


Figure 3: **Half-life replenishment factor evolution.** The fraction of mass that has been accreted in the last half of the disc life-time, $f_{M,1/2}$, as a function of time for 500 discs. On the left, we show the time evolution of $f_{M,1/2}$ for a random subset of 100 discs for clarity. These lines are coloured by the ratio of the disc mass to stellar mass M_{disc}/m_* , shown in the colour bar along the top. On the right hand side we show a cumulative fraction for $f_{M,1/2}$ at 1, 2, 3 and 8 Myr. Only discs with a total mass $M_{\text{disc}} > 3 \times 10^{-5} M_{\odot}$ are included in this cumulative fraction, lower mass discs are assumed to be dispersed.

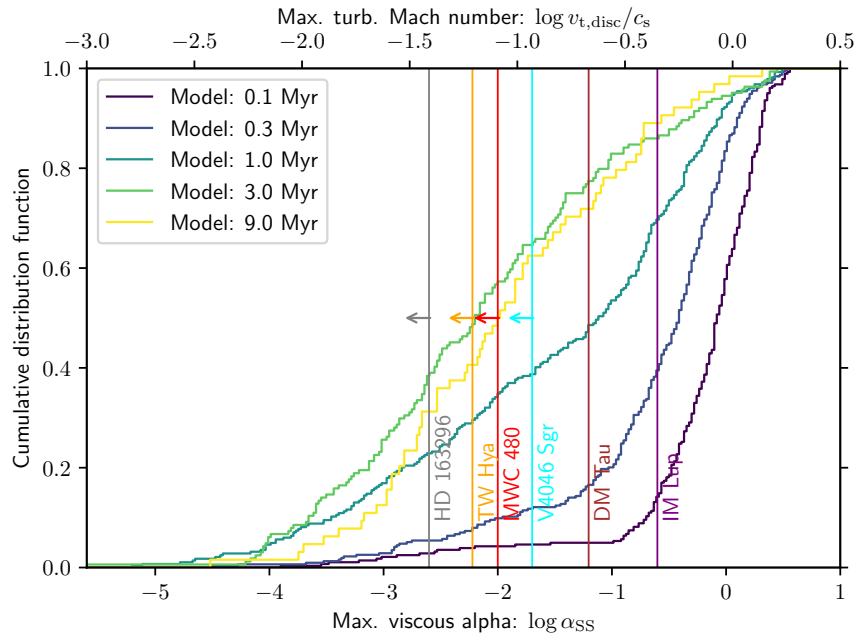


Figure 4: **Turbulent viscosity driven by in-fall.** Evolution of the cumulative distribution function for the turbulent Mach number (or viscous α_{SS} , top axis) for the discs in our model, assuming a maximal energy input efficiency $\epsilon_t = 1$. Each line colour represents a different disc age in our model, from 0.1 to 9 Myr. We show as coloured vertical lines some examples of discs with constraints on their turbulent velocity from the literature, several of which are upper limits.⁷

METHODS

Overview: Our aim is to estimate the distribution of accretion histories for a population of young stars that resembles those surveyed for disc properties in the solar neighbourhood. To do so, we must follow the density and relative velocity of gas surrounding these young stars. This includes both the period in which it is bound to the gaseous overdensity in which it forms,³⁶ and once the bound gas has dispersed. The most direct approach would be to perform full hydrodynamic simulations of star formation in the turbulent interstellar medium within the galaxy. This would require capturing star formation physics over a wide range of scales, maintaining the turbulent cascade that propagates from the galactic^{37,69,70} down to the protoplanetary disc size scale for the several Myr over which protoplanetary discs persist. This is computationally challenging, if not impracticable. However, we can still estimate the statistical evolution of the accretion rate semi-analytically by applying an excursion set formalism.³⁹ This method is effectively zero dimensional, and is therefore a highly efficient way of statistically following density fluctuations of the ISM.

We adopt the following approach:

1. *Properties of local star forming regions:* Apply the excursion set formalism to determine the typical properties of star forming regions that are targeted for local disc surveys (within ~ 200 pc).
2. *Collapse of the molecular cloud:* Adopt a simple model for the collapse of these star forming regions, and the rate at which stars form as a function of time.

3. *Stellar dynamics in the bound cloud:* Draw a representative stellar population, using the star formation rate based on step 2 to statistically calculate when stars should form during the collapse of a region. Compute the dynamical evolution of these stars under the cloud potential until cloud dispersal, tracking the local gas density and velocity.
4. *Evolution of the turbulent medium:* Compute the time-evolution of the turbulent medium outside of the bound star forming region, using the same approach as in step 1, to continue to track the local density and velocity after the exhaustion of the bound gas reservoir (star forming region).
5. *Accretion rate onto the star-disc system:* Calculate the Bondi-Hoyle-Lyttleton (BHL) accretion rate onto the star-disc system over time.
6. *Disc properties:* Couple the external accretion rate to a simple model including accretion onto the host star, to track the evolution of the disc masses, radii, turbulence and stellar accretion rate.
7. *Observational comparison:* Compare the resultant model to observed disc properties.

In the remainder of this work, we describe these steps in greater detail. We then delve deeper into some of the implications of our model.

Properties of local star forming regions (step 1): In the first instance, we wish to quantify the properties of giant molecular clouds (GMCs) that undergo gravitational collapse to form stars. This can be reframed in terms of quantifying the maximum turbulent size-scale on which a given

volume of space in the mid-plane of the galaxy is marginally gravitationally unstable at any given time. All scales smaller than this size-scale will also be bound to this cloud, and therefore this can be considered a unit of star formation, or a star forming region. The problem of quantifying the mass or radius distribution of collapsing star forming regions can be solved via excursion set theory, as has been successfully applied to dark matter halos.³⁸

We follow Hopkins (2012),³⁹ who applied the excursion set formalism in the context of GMCs in the galactic disc. The approach can be summarised as follows, but we refer the interested reader to that work for greater detail. Most generally, it is clear that the density of gas on any given scale can be described as the sum of the contributions to this density at all larger scales. Supersonic turbulence yields a log-normal probability distribution in volume space for the gas density, with a dispersion that is dependent on the local Mach number.⁷¹ Therefore, dispersion in the contribution of any range of scales to the deviation from the median depends on the turbulent velocity on that scale. In a supersonic, rapidly cooling medium, the cascade of energy from large scales to small scales produces an energy spectrum with power-law exponent $p = 2$, or turbulent velocity that scales with the square-root of the size-scale.⁷² The critical density required for collapse at any intermediate size-scale is then related to the effective pressure support afforded to the medium from the turbulent motions on that scale, via the dispersion relation for a disc of a finite thickness.⁷³ On the largest scales, this pressure support effectively comes from galactic shear, while on the smallest scales, turbulent fragmentation can be suppressed by the thermal pressure.⁷⁴ In principle, the influence of magnetic fields can also be accounted for in this context, but Hopkins (2012) notes that this modification practically amounts to changing the sound speed, with only minor quantitative

consequences for our model. In the context of the BHL accretion rate that we eventually compute, modifications of only a factor of order unity are expected due to local magnetic fields.^{75,76} Given the turbulent energy spectrum, a ‘trajectory’ in logarithmic density space can be instantaneously defined as the cumulative sum of perturbations from the largest to smallest scales. For any trajectory, a gravitationally unstable GMC, or star forming region, is defined on the largest length scale which is unstable (if any), all smaller length scales being subsumed within the larger volume.

In our case, we follow similar parameter choices to those adopted by Hopkins (2012). The energy spectrum normalisation is defined such that the velocity dispersion at the scale height h of the gaseous galactic disc $\sigma_g(h) = h\Omega = 6 \text{ km s}^{-1}$, where $\Omega = 2.6 \times 10^{-2} \text{ Myr}^{-1}$. We assume a surface density of the galactic disc in the solar neighbourhood $\Sigma = 12 M_\odot \text{ pc}^{-2}$, yielding a Toomre $Q = 1.33$. We always assume a sound speed $c_s = 0.2 \text{ km s}^{-1}$ and define a grid with a maximum scale $R_{\text{max}} = 5h$ down to a minimum scale $R_{\text{min}} < 0.01 \text{ pc}$, each grid cell being 95 percent of the spatial scale of the previous cell.

Finally, to define the absolute frequency of star forming regions within a certain age range in the solar neighbourhood depends on the turbulent time-scale. This is itself a function of spatial scale:

$$\tau_t(R) = \eta t_{\text{cross}} = \eta R / \langle v_t^2(R) \rangle^{1/2}, \quad (3)$$

where t_{cross} is the crossing time-scale and $\eta \approx 1$.⁷⁷ An appropriate time-scale $\tau_{t,0}$ over which the trajectory ‘resets’ corresponds to the turbulent time-scale on the scales that dominate density variations. We therefore estimate $\tau_{t,0} \approx \tau_t(h)$. We can then estimate the differential number of star

forming region younger than a certain age $\Delta\tau$ within a given volume ΔV :

$$\left\langle \frac{dN}{dM} \right\rangle \approx \frac{1}{2^3} \frac{\Delta\tau}{\tau_{t,0}} \frac{\Delta V \rho}{M} \cdot \frac{N_{\text{coll}}}{N_{\text{traj}}} \quad (4)$$

where N_{coll} is the number of unstable trajectories from a sample of N_{traj} . We include a factor $1/2^3$ since given a region of radius R_{SFR} , any other region with R_{SFR} is forbidden inside a distance of $2R_{\text{SFR}}$ (such a region would merge with the original region). In the averaging for equation 4 we have ignored an obvious consequence of the random walk. That is that the unstable regions should be spatially correlated, since clouds preferentially collapse in regions of high density at spatial scales larger than the nascent star forming region. However, Hopkins (2012) find that there is little bias for the low mass star forming regions, with $R_{\text{SFR}} \ll h$. These are the regions relevant for our analysis.

We show the outcome of this calculation for 10^5 independent trajectories in Figure Extended Data Figure 1. We plot the number of star forming regions above a given mass M within a spherical volume with radius $R_{\text{obs}} = 200$ pc younger than 10 Myr. This is approximately the radius within which the majority of protoplanetary disc statistics have been compiled,⁴² and the dispersal time-scale for protoplanetary discs.^{1,78} We define the mass threshold below which we expect > 10 star forming regions to be the threshold for being well sampled. This yields a mass limit $M_{\text{local}} \approx 500 M_{\odot}$. Note, our definition of a star forming region is a region that is collapsing to form stars. This is in contrast to a broader complex that may not be collapsing globally. As an illustrative example, the Taurus-Auriga association has a total mass much larger than $500 M_{\odot}$.⁶⁸ However, the complex as a whole is not collapsing to form stars. Instead collapse and star formation has occurred in several smaller sub-regions. It is these regions, or ‘NESTS’,⁷⁹ that are the individual

star forming regions in the sense appropriate to this work. In Taurus, these regions are typically a few tens of solar masses. The older region Upper Scorpius has a total stellar mass $\sim 1400 M_{\odot}$,⁸⁰ but is also composed of several individual populations.⁸¹ The nearest individual star forming region with total mass of several $10^3 M_{\odot}$ is the Orion Nebula cluster,⁸² at a distance of ~ 400 pc.⁸³ We conclude that, although our approach is approximate in that it neglects some physical processes that may influence local star formation, such as possible nearby supernovae,⁸⁴ the upper mass limit we infer is reasonable. Our subsequent results do not depend strongly on this limit, as long as we exclude much more massive regions that may be dispersed prematurely by stellar feedback.

Motivated by this result, hereafter we will truncate the GMC mass function above $500 M_{\odot}$. We will also exclude regions with masses $< 10M_{\odot}$, for which we expect the turbulent velocity to approach the sound speed ($\mathcal{M} \sim 1$). In principle, they may still be accurately sampled by the excursion set formalism if the density distribution does not diverge greatly from log-normal. However, we cannot choose an arbitrary small lower mass limit, since for much lower mass regions there is insufficient mass to form stellar mass objects. Experimentation shows that our results are not strongly dependent on our choice of lower mass limit.

Collapse of the giant molecular cloud (step 2): In the early stage after a star forms, it occupies the local star forming region that is undergoing gravitational collapse. Since we are interested in the local density and velocity evolution throughout a star's lifetime, we require a simple model to follow the collapse of the GMC and formation of stars. Once the GMC becomes gravitationally unstable, it collapses on a free-fall time-scale. It does not do so monolithically, but because smaller

sub-regions of the cloud may be higher density (and therefore have shorter free-fall time-scales), they fragment first and continue to accrete from their parent structures.⁸⁵ Simultaneously, the cloud is exposed to heating by feedback processes from the stars as they form. A wide range of analytic and semi-analytic approaches have been developed to describe this process.⁸⁶ We are helped in this context in our interest in low mass star forming regions that are locally well sampled. Since we do not expect many massive stars or supernovae among these local regions, we will hereafter ignore feedback processes and exclusively consider gravitational collapse.

We adopt the approach of Girichidis et al. (2014)⁴⁰ in modelling the rate of star formation during the collapse of the GMC. The approach of those authors is attractive for its simplicity, while also retaining a self-consistent treatment of the gas density distribution as it evolves under gravity. We briefly review the approach here, referring the reader to the original work for details.

We consider a spherical region undergoing free-fall collapse from rest, which may be contained within a larger gravitationally unstable cloud. Girichidis (2014) wrote an invertible, analytic approximation for the density of such a region as a function of time. Given an analytically integrable initial density distribution, there is a corresponding analytic expression for the fraction of an initial gas reservoir that collapses beyond any given threshold as a function of time. The initial density distribution in our collapsing region is log-normal, with a dispersion determined by the Mach number on the scale of collapse. We choose the critical density to be such that the local free-fall time is shorter than 0.1 Myr. Given the accelerating nature of gravitational collapse, the exact threshold time is irrelevant so long as it is substantially shorter than the time-scale for the

global collapse of the star forming region. The star formation rate is defined to be the rate at which material crosses this threshold density. We assume the cloud is instantly dispersed on cessation of the star formation phase, which continues until a star formation efficiency $\epsilon = 0.5$ is reached, this value being commensurate with simulations of stellar core formation.⁴¹ We expect stellar feedback, which we do not consider and may shut off star formation in massive clouds, to have a negligible influence on the low mass star forming regions that are our focus. High star formation efficiencies similar to those we assume are also reached for more sophisticated models of star formation in a collapsing cloud for low mass clouds.⁸⁶

Stellar dynamics in the bound cloud (step 3): Having defined a local star formation rate, we can draw formation times for an initial stellar population. Since these stars are initially bound to the cloud from which they form, we integrate the orbit of the star within the gravitational potential of the cloud, ignoring interactions with other stars. For convenience we will consider a Plummer potential with a core radius $a = R_{\text{SFR}}/2.6$, such that the outer radius of the star forming region is twice the half-mass radius. Stars are drawn from within the core radius, and we draw an isotropic velocity distribution with a dispersion assuming instantaneous virial equilibrium with the cloud. To track local density and relative velocity of the gas, we assume a static, smooth Plummer density profile.³⁶ We then evolve the star under the potential, varying the core radius as the spherical star forming region contracts until the final dispersal of the cloud (when $M_* = \epsilon M_{\text{tot}}$).

Evolution of the turbulent medium (step 4): Throughout the evolution of the cloud, we continue to track the local density and velocity evolution of the background ISM. We do this once again fol-

lowing the procedure of Hopkins (2012). We assume the turbulence is globally steady-state, such that the turbulent velocity cascade is maintained outside of the collapsing regions. The probability density function for any Gaussian random variable δ under these conditions obeys a generalized Fokker-Planck equation. We can therefore redefine our trajectory at $t + \Delta t$ by computing a random walk step:

$$\Delta\delta_j(t + \Delta t) = \Delta\delta_j(t) \exp(-\Delta t/\tau_t) + \mathcal{R} \sqrt{\Delta S (1 - \exp(-2 \Delta t/\tau_t))}, \quad (5)$$

where \mathcal{R} is a Gaussian random number with unity variance. The new trajectory is the sum of the components given by equation 5. We define the time-step to be 2 percent of the shortest turbulent time-scale in our grid. We evolve the ISM throughout the bound phase of star formation, but only use it to compute accretion rates after the dispersal of the cloud.

Equation 5 applies both to the logarithmic density perturbations and to each component of the interstellar gas velocity. The relative velocity of the star as it moves through the unbound density field after the dispersal of the cloud is then the gas velocity at the relevant scale, minus the velocity of the star with respect to the bound cloud at the time of dispersal and the velocity of the cloud itself. The velocity of the cloud is fixed as the gas velocity at the time and scale of cloud collapse.

Accretion rate onto the star-disc system (step 5): Bondi-Hoyle-Lyttleton (BHL) accretion has been the topic of many works.³⁴ In the purest case, it is the gravitational focusing of the test particles (representing the ISM), resulting in a stagnation point in the wake of the star within which material is accreted. The instantaneous Bondi-Hoyle-Lyttleton (BHL) radius within which

material is captured is then defined:

$$R_{\text{BHL}} = \frac{2Gm_*}{(c_s^2 + \Delta v_{\text{gas}}^2)}. \quad (6)$$

Streamlines with an impact parameter at the BHL radius R_{BHL} hit a stagnation point along the axis coincident with the relative upstream gas velocity vector. In the ideal case, in an homogeneous medium, they then accrete directly onto the star.

If the tidal radius $R_{\text{T}} < R_{\text{BHL}}$, then this radius limits the material that can be captured by the star. If a star is bound to a mass M_{b} at a radius r_{b} , then:

$$R_{\text{T}} = r_{\text{b}} \left(\frac{m_*}{3M_{\text{b}}} \right)^{1/3}. \quad (7)$$

Initially, this radius is determined by the collapsing cloud, where r_{b} is the instantaneous location of the star with respect to the centre of the region. Once the cloud has dispersed, we take the galactic values $r_{\text{b}} = 8 \text{ kpc}$ and $M_{\text{b}} = 10^{12} M_{\odot}$. The accretion radius also cannot exceed the turbulent size scale under consideration, R_{t} . Thus the accretion radius can be defined:

$$R_{\text{acc}} = \min \{R_{\text{BHL}}, R_{\text{T}}, R_{\text{t}}\}. \quad (8)$$

Material within the cross-section carved out by this radius is captured by the star. At any turbulent scale, we can estimate the instantaneous rate at which a star captures material in such a scenario:^{33,87}

$$\dot{M}_{\text{BHL}} \approx \pi R_{\text{acc}}^2 \rho (\lambda c_s^2 + \Delta v_{\text{gas}}^2)^{1/2}, \quad (9)$$

where $\lambda = e^{3/2}/4 \approx 1.12$ in the isothermal limit. Material is accreted on the turbulent scale that maximises the accretion rate according to equation 9. We therefore define the ambient gas density

ρ_{gas} and relative velocity Δv_{gas} to correspond to the quantities on this accretion scale. Before the dispersal of the formation cloud, the density and velocity are defined at the location of the star from the appropriate Plummer profile.

It is now necessary to define the mass of a star to calculate accretion rates. Hereafter, stellar masses are always drawn from a log-uniform distribution between $0.01 - 3 M_{\odot}$. This distribution is not important because we will resample when comparing to observations, except that we need to fully sample the stellar mass range relevant for drawing comparisons to protoplanetary disc surveys. Although the stellar masses do not evolve self-consistently as the stars accrete in our model, the total mass that they would gain is nearly always a small fraction of the initial stellar mass. We then draw 500 accretion histories from a representative sample of synthetic star forming regions, with a draw probability weighted by the stellar mass of the region.

We show the outcome for the evolution of the local density, relative velocity and BHL accretion rate (normalised to show the accretion rate assuming a solar mass star) for a subset of six stars in Figure 1. Given that density in particular can vary over several orders of magnitude, we also draw an approximate comparison to the typical densities in observed star forming regions. To do so, we adopt averaged density estimates from Table 4 of Goldsmith et al. (2008)⁶⁸ for a number of high density areas within the Taurus star forming complex. We convert the mass estimates M_{enc} within the quoted surface area A_{surf} to a density estimate by approximating spherical geometry, such that the volume averaged density is:

$$\langle \rho_{\text{enc}} \rangle_V \sim \frac{3M_{\text{enc}}}{4\pi(A_{\text{surf}}/\pi)^{3/2}}. \quad (10)$$

However, this approximation probably yields an underestimate of the typical density within or close to collapsing star forming regions. This is because the area A_{surf} as defined by Goldsmith et al. is not limited to a single, collapsing star forming region. Instead, it contains both high and low density subregions, resulting in an underestimate of $\langle \rho_{\text{enc}} \rangle_V$ for the collapsing regions. Nonetheless, the typical $\langle \rho_{\text{enc}} \rangle_V \sim 3 \times 10^{-21} \text{ cm g}^{-3}$ is commensurate with the high-end for the local gas densities implied by our model (see the middle panel of Figure 1). We conclude that the local densities for stars in our model are broadly consistent with the those observed in local star forming regions.

Disc properties (step 6): BHL accretion in a turbulent medium is unlikely to result in accretion directly onto the star. In an homogeneous medium the velocities of streamlines are zero at the stagnation point. Captured material therefore has zero angular momentum and accretes directly onto the star. However, in an inhomogeneous medium, vorticity results in retention of a bound disc structure that does not instantly accrete onto the star.⁴³ For a given fluid element, we may then expect accretion onto the star to be mediated via a protoplanetary disc.^{66,88}

We now aim to generate a simplified ‘population synthesis’ of discs shaped by BHL accretion. To do so, we wish to initially remain agnostic as to the driver of stellar accretion.^{89,90} We therefore consider a stellar accretion rate $\dot{M}_{\text{acc}} = M_{\text{disc}}/\tau_{\text{acc}}$, for disc mass M_{disc} and fixed accretion time-scale τ_{acc} . For each of the discs in our sample discussed, we solve the initial value problem:

$$\dot{M}_{\text{disc}} = \dot{M}_{\text{BHL}} - \dot{M}_{\text{acc}}. \quad (11)$$

To evolve the disc mass, in our fiducial model we fix the initial $M_{\text{disc}}(t = 0) = 0$. This is

equivalent to the assumption that the initial disc that forms due to core collapse is low mass, or rapidly depleted. This runs counter to the conventional assumption that the protoplanetary disc represents an evolved state of the primordial protostellar disc, which formed during the stellar core collapse. We make this decision as a ‘clean’ test of our model; we wish to explore the properties of discs arising from BHL accretion alone. Such a model requires no additional free parameters. We emphasise that no specific observational constraints contradict a low initial disc mass. Any such evidence would need to connect the primordial circumstellar material, which forms over $\sim 10^2$ years, to the protoplanetary disc, which in the context of this work forms over $\sim 10^5$ years and evolves over $\sim 10^6$ years. Although (massive) discs around Class 0 stars have been inferred,^{27,91} interpreting these observations in terms of the exact age of the (proto-)star (down to $\sim 10^4$ years), the nature of the disc and the time-scale over which any such disc should survive is not simple. Since few, if any, unambiguous observations exist constraining the properties of primordial discs that are categorically around stars of age $\ll 10^5$ years, there is no reason to assume that such a primordial disc should be both long-lived and comparable in mass to the subsequently accreted one. Indeed, it would be a remarkable coincidence if BHL accretion and protostar formation contribute an equal fraction of mass to the disc population. Nonetheless, we also explore the impact of this assumption on our results below.

For $\tau_{\text{acc}} = M_{\text{disc}}/\dot{M}_{\text{acc}}$ we assume a log-uniform distribution ± 1 dex around $\log \tau_{\text{acc}}/1 \text{ Myr} = -0.5$, based on visual inspection of the observed distribution.⁴⁴ Empirically, the time-scale τ_{acc} is not strongly correlated with stellar mass, but may be a complex function of the disc properties or stellar age. For example, visually interpreting Figure 12 of Almendros-Abad et al. (2024),⁴⁴ the

median accretion time-scale appears to be $\tau_{\text{acc},1/2} \sim 0.1$ Myr for the young region ρ Ophiuchus, while $\tau_{\text{acc},1/2} \sim 1$ Myr for the older Lupus region. Indeed, we expect rapid BHL accretion to instigate turbulence in the disc, temporarily decreasing τ_{acc} . However, empirically it is not clear the degree to which any variation of τ_{acc} is a survival bias, discs with shorter τ_{acc} having been depleted (we will show a similar evolution in our model which has fixed τ_{acc} for each star below). While exploring time- or accretion-dependent τ_{acc} is an interesting avenue for future exploration, we initially maintain our simplified model, subsequently exploring the potential role of the ISM in driving a time-dependent stellar accretion rate.

Given the initial condition and accretion time-scale, we evolve each disc mass according to equation 11 over the entire time period under consideration. However, we assume a simple criterion for disc dispersal: $M_{\text{disc}} < 3 \times 10^{-5} M_{\odot}$. We adopt this criterion when showing disc properties in subsequent analysis. This threshold is motivated empirically by the fact that few discs have masses below this value; our results are not strongly sensitive to this choice within a sensible range.

Observational comparison (step 7): We wish to compare our model to observed discs with comparable stellar ages. The ages of star forming regions can both be observationally uncertain⁹² and should exhibit physical scatter given the finite duration of the star formation process. However, nominally ages for the youngest populations of stars in the ρ Ophiuchus complex are $\sim 0.1 - 1$ Myr,⁹³ in Taurus are $\sim 1-3$ Myr,⁹⁴ in Lupus are $\lesssim 3$ Myr,⁹⁵ in Chameleon I have been estimated at $\sim 1-2$ Myr⁹⁶ and $\sim 3-6$ Myr,⁹⁷ and Upper Sco are $\sim 5 - 10$ Myr.^{98,99} We compare these regions to our model at ages, 0.5, 1, 2, 3 and 5 Myr respectively; these choices should be

considered illustrative, not precise. For total disc masses we take $M_{\text{disc}} = 10^2 M_{\text{dust}}$, where M_{dust} is as quoted by Manara et al. (2023),⁴² inferred from the mm continuum flux with standard assumptions for opacity and temperature. In order to draw comparisons with each, we perform a Gaussian kernel density estimate with Scott’s rule for bandwidth selection.¹⁰⁰ Where we compare to data directly, we weight the model data points to yield the same distribution in the stellar mass axis as for the observational dataset. In practice, this means dividing the stellar mass distribution into bins, and defining the weight of model data points in each bin i to be $N_{\text{obs},i}/N_{\text{mod},i}$, where $N_{\text{obs},i}$ and $N_{\text{model},i}$ are the number of observed and model points in bin i respectively. The results of these comparisons are shown in Figure 2 and discussed in the main article, however we make some additional comments on the disc properties here as follows.

Disc masses: Disc masses are possibly the best metric of success of a disc evolution model, since they are time-integrated (i.e. not sensitive to temporal fluctuations) and relatively straightforwardly defined, albeit with some uncertain factors and observational caveats. Surveys inferring dust mass via mm flux are also relatively complete for several local star forming regions. In the top row of Figure 2, disc masses from our model show remarkable agreement with the observed data at all ages. Disc masses from our model fill-out the observed ‘wedge’ in the $m_* - M_{\text{disc}}$ plane.

We show the time evolution of the disc mass distribution in our model more quantitatively in Extended Data Figure 3, where we plot the cumulative distribution function for disc masses around stars $0.5 M_{\odot} < m_* < 1 M_{\odot}$. We also show observed distributions for Taurus and Upper Sco, leaving out the other regions for clarity. We can see that at ~ 1 Myr, the disc mass distribution in our

model is very similar to the distribution in Taurus. This decreases after a few Myr until reaching a similar distribution to that seen in Upper Sco between 3 and 9 Myr. Within uncertainties, and given the caveat of a range of stellar ages in each region, our model appears fully consistent with the observed disc mass distributions. More speculatively, we note that the disc takes ~ 0.3 Myr to reach the maximum mass distribution. This is interesting in the context of ρ Ophiuchus, which have discs that are more compact^{45,46} and lower mass^{47,101} than $\sim 1-2$ Myr old regions. A similar result has been found in Corona Australis.¹⁰² Our models suggest that this is plausibly the result of ongoing mass assembly proceeding from outside-in, via BHL accretion.

Stellar accretion rates: The accretion rates from our model are entirely determined by the disc mass distribution, since we have imposed $\dot{M}_{\text{acc}} \propto M_{\text{disc}}/\tau_{\text{acc}}$. They are therefore not an independent test of our model, but a validation or repudiation of this assumption. Given that we have anchored τ_{acc} to observations, and we have found observational agreement with the disc mass distribution, as expected we also find for the majority of regions we have excellent agreement for accretion rates (middle row, Figure 2). We note minor tension particularly in the case of Chameleon I, for which some accretion rates are somewhat larger than predicted by our model. This is plausibly the result of a younger population than the comparison age we have adopted. For example, Galli et al. (2021)⁹⁶ argue that the older estimate obtained by Luhman et al. (2007)⁹⁷ may be explained by systematic distance underestimate (then Chameleon I may be $\sim 1-2$ Myr old). Overall, we find excellent agreement between stellar accretion rates in our model and the observed samples. Since our model does not contain any stellar mass dependent disc physics (except the BHL accretion rate), this makes a strong argument in favour of BHL accretion as the origin of disc assembly.

We may also ask whether the data supports our assumption of a fixed τ_{acc} distribution with stellar mass and time. It is possible, even probable, that this accretion time-scale does vary over time, particularly if internal disc turbulence is driven to some degree by the material inherited from the ISM (which is plausible, see Figure 4). As previously discussed, empirically there is some variation in τ_{acc} between regions.⁴⁴ In this case, the true distribution of τ_{acc} may be a function of the state of the ISM in each specific region. However, even for fixed τ_{acc} for individual stars, the fact that star-disc systems with shorter τ_{acc} lose their discs earlier mean that they drop out of the sample of surviving discs. For our model, this is shown in Extended Data Figure 4, where we find that once discs are ~ 3 Myr old, the median $\tau_{\text{acc}} \sim 1$ Myr, a factor three larger than for the initial disc population. This moderate increase is similar to the median for the observed distribution for discs of this age.⁴⁴ We conclude that, while τ_{acc} may vary over time for individual stars, such temporal variation is not required to produce the observed disc population.

Outer radii: We can also consider the distribution of gaseous disc radii R_{disc} we infer from our model. However, the appropriate definition of R_{disc} is less clear than for disc masses or stellar accretion rates in terms of the correspondence between the model and observational data. The observed outer radius in dust is dependent on variations in the dust opacity¹⁰³ and in gas molecular tracers, such as CO, outer radii are dependent on thermochemistry.¹⁰⁴ Both are dependent on the definition of ‘outer radius’, often defined by the radius that encloses some fraction of the total flux. In our simple models, we do not explicitly define an outer radius. A sensible estimate for R_{disc} is the accretion radius R_{acc} at the most recent time for which the disc is accumulating mass (i.e. $\dot{M}_{\text{BHL}} > \dot{M}_{\text{acc}}$), and this is the definition we adopt in this work and in constructing Figure 2.

In the absence of other disc evolution processes, such as viscous spreading,⁸⁹ we actually expect $R_{\text{acc}} > R_{\text{disc}}$, since the outer radius depends on the fraction of residual angular momentum from the accreted ISM. With these caveats, we proceed with the assumption $R_{\text{acc}} \approx R_{\text{disc}}$ in our comparison with observations in the main article.

Disc lifetimes: For a fair comparison of disc property distributions, we must also confirm that the total fraction of discs included in our sample is similar in our model to those in star forming regions of a given age. We therefore show the disc fraction as a function of time in Extended Data Figure 2, by the definition $M_{\text{disc}} > 3 \times 10^{-5} M_{\odot}$. We confirm that our model yields reasonable disc fractions over the range of times we consider in our disc property comparisons. We find a very similar disc fraction evolution to the exponential decay relationships suggested in the literature, typically with dispersal time-scale $\tau_{\text{disc}} \sim 3\text{--}5$ Myr.^{1,105}

Interestingly, we find that the initial disc fraction is not 100 percent in our model, but is maximal at ~ 85 percent. This appears to be consistent with observations which indicate that, even for very young disc populations, the disc fraction never exceeds ~ 80 percent.¹⁰⁶ However, when accounting for close binaries, this fraction could be closer to 100 percent for single stars.¹⁰⁷ The model prediction of a somewhat suppressed initial disc fraction should therefore not be interpreted as a unique signature of BHL accretion, and may also depend on the presence or absence of a primordial disc. We also find a somewhat flatter disc fraction as a function of time than a simple exponential decay with linear time exponent. Some authors to suggest such a flattened functional form for the disc fraction,⁷⁸ supported by a non-negligible disc fractions in clusters that are tens of

Myr old.¹⁰⁸ Such surviving discs can be easily understood in the context of the stochastic accretion process that defines our model.

We caveat this discussion in that we have not included any end-stage disc dispersal processes; in particular the photoevaporative wind driven by the central star.^{109–113} We would expect that, at least for very low mass discs, mass-loss may be dominated by such a wind. Our assumption is effectively that mass-loss in the wind is inefficient; in this case we can assume that the lifetime of an observable disc is essentially set by the accretion process in isolation. Once a disc is ‘dispersed’ in our model, if at some later stage the disc replenishment occurs more rapidly than the true photoevaporation rate, then our model remains valid. Nonetheless, a future investigation of how photoevaporation may interact with BHL accretion for disc populations is warranted in future work.

Replenished mass fraction: As discussed in the main article, it is not clear immediately from Figure 2 whether disc properties are set by a continuous process of BHL accretion. Does BHL just set the initial disc properties that then simply evolve over our imposed time-scale τ_{acc} , or is disc material constantly replenished over the disc lifetime? This is an important distinction because if disc material is constantly being replenished then, even with well-determined initial conditions, the distribution of disc properties can never be a direct probe of isolated disc evolution.

To understand what fraction of material in observed discs should originate from ‘fresh’ ISM material, we define a metric $f_{M,1/2}$ to be the ‘half-life replenishment factor’. That is, the fraction of material within the disc that has been accreted within the most recent half of the disc life-time.

In the absence of BHL accretion, equation 11 has a trivial analytic solution that we label $M_{\text{isol}}(t)$, given an initial mass. Then, if stellar accretion of the older material occurs before the accretion of younger material, and if stellar accretion is the only mechanism by which mass is removed from the disc, then at time t_2 the fraction of mass that has been added to the disc since time t_1 is

$$f_M(t_1|t_2, M_{\text{disc}}(t_2)) = 1 - M_{\text{isol}}(t_1|t_2, M_{\text{disc}}(t_2))/M_{\text{disc}}(t_1). \quad (12)$$

From equation 12 we define $f_{M,1/2}$ such that $t_2 = t_1/2$. We expect this estimation of $f_{M,1/2}$ to be a lower bound because we ignore any other disc dispersal processes. Processes such as planet formation or disc winds should be expected to reduce M_{isol} , thus increasing f_M .

Applying this metric in Figure 3, we find a substantial fraction of discs composed of a high proportion of recently captured ISM material. We therefore conclude that disc properties are constantly ‘reset’. This would suggest that the distributions of observed disc properties should not be used to test of theoretical models for isolated disc evolution.

Sensitivity to the initial disc mass: In drawing the above conclusions, we have made the assumption that the initial disc mass is negligible compared to the subsequently accreted material. As discussed, this assumption is justified in the desire for a ‘clean’ test of the disc properties resulting from BHL accretion, retaining a simple model with few free parameters, and by the coincidence that an alternative would imply. However, given that this assumption is also unconventional, we can ask whether our conclusion regarding the degree of disc replenishment holds in the event of the coincidence that the primordial disc mass is comparable to the subsequently captured mass.

To investigate the sensitivity of our conclusions on disc replenishment to this assumption, we repeat our calculations with disc masses initially similar to the observed distribution in young star forming regions. In practice, we adopt a log-normal distribution for the disc mass with 1 dex of scatter around the relationship

$$M_{\text{disc}}(t = 0) = 0.01 \left(\frac{m_*}{1 M_{\odot}} \right)^2 M_{\odot}. \quad (13)$$

We show the resultant disc properties in Extended Data Figure 5, which again are in good agreement with the observed disc properties. Our adopted initial disc masses are approximately the maximum we could adopt while still remaining consistent with the observed distribution of disc masses. The outcome for the half-life disc replenishment factor is shown in Extended Data Figure 6. Although in this case $f_{M,1/2}$ is somewhat reduced early on in the disc evolution, overall differences in the distribution over time is minor. The fraction of discs with at least some recently accreted material remains similar, while we find that $f_{M,1/2} \sim 0.2\text{--}0.45$ throughout the disc lifetime. Therefore, even under the assumption that the primordial disc is coincidentally similar in mass to the subsequently accreted one, and ignoring all internal depletion processes, we still expect a substantial fraction of discs to be composed of recently captured disc material. Our conclusion that the present day disc properties are not a good probe of internal disc physics therefore appears robust.

Disc turbulence and angular momentum transport: In our model, we have assumed that disc mass is accreted onto the star with a fixed time-scale τ_{acc} via an undefined angular momentum transport process. This process could be internal to the star-disc system, driven by magnetic winds or due to (magneto-)hydrodynamic instability.^{67,90} However, the ISM itself could also be the origin

of protoplanetary disc turbulence. The degree to which angular momentum transport is mediated by turbulence remains an open question, but measurements indicate it could be the origin of stellar accretion in at least some discs.⁷

To estimate the degree of ISM-induced turbulence, we must compute the balance between the rate at which energy is deposited compared to the decay of that turbulent energy. The rate at which energy decays is:³⁷

$$\dot{E}_{\text{decay}} = -\frac{1}{2} \frac{M_{\text{disc}} v_{\text{t,disc}}^3}{H_{\text{disc}}}, \quad (14)$$

where $H_{\text{disc}} \sim 0.1R_{\text{disc}}$ is the disc scale height. The in-flowing turbulent energy from the ISM is:

$$\dot{E}_{\text{in}} = \frac{1}{2} \dot{M}_{\text{BHL}} v_{\text{in}}^2. \quad (15)$$

If the velocity of the flow is dominated by the gravitational acceleration from the central star, then:

$$v_{\text{in}}^2 \approx \frac{2Gm_*}{R_{\text{disc}}}. \quad (16)$$

Then, if the fraction of the energy that goes into turbulent motion in the disc is $\epsilon_t = |\dot{E}_{\text{decay}}/\dot{E}_{\text{in}}| \leq 1$ and the disc is in a steady state, then (rewriting equation 30 of Klessen & Henebelle 2010³⁷):

$$\left(\frac{v_{\text{t,disc}}}{c_s}\right)^3 \approx \frac{2\epsilon_t}{3^{3/2}} \left(\frac{c_s}{0.2 \text{ km s}^{-1}}\right)^{-3} \left(\frac{\dot{M}_{\text{BHL}}}{1.9 \times 10^{-8} M_{\odot} \text{ yr}^{-1}}\right) \left(\frac{M_{\text{disc}}}{10^{-2} m_{\star}}\right)^{-1} \left(\frac{H_{\text{disc}}}{R_{\text{disc}}}\right). \quad (17)$$

Instantaneous steady state is probably a good approximation, because the decay timescale is

$$\tau_{\text{decay}} = |E_{\text{t,disc}}/\dot{E}_{\text{decay}}| = H_{\text{disc}}/v_{\text{t,disc}} \ll \tau_{\text{disc}}, \quad (18)$$

where

$$E_{\text{t,disc}} = \frac{1}{2} M_{\text{disc}} v_{\text{t,disc}}^2. \quad (19)$$

Therefore, the BHL accretion rate \dot{M}_{BHL} needs to remain sufficient to drive observed turbulence throughout the disc lifetime. However, this requirement is probably met for most discs in the context of our model. With the exception of DM Tau, which has turbulent velocity $v_{\text{t,disc}} \sim 0.25\text{--}0.33 c_s$, and IM Lup which has $v_{\text{t,disc}} \sim 0.4\text{--}0.6 c_s$,⁶⁰ attempts to measure turbulence in protoplanetary discs have resulted in upper limits. For example, for the disc around HD 163296 this upper limit is $v_{\text{t,disc}} \lesssim 0.05 c_s$,^{56,114} and for TW Hydra it is $v_{\text{t,disc}} \lesssim 0.08 c_s$.^{54,115} For $M_{\text{disc}}/m_* = 0.01$, $H_{\text{disc}}/R_{\text{disc}} = 0.1$ and $\epsilon_t = 1$, then even substituting a modest $\dot{M}_{\text{BHL}} \sim 10^{-11} M_{\odot} \text{ yr}^{-1}$ yields $v_{\text{t,disc}} \sim 0.03 c_s$, similar to the empirical upper limit on turbulence in some discs. This is approximately the median BHL accretion rate for a solar mass star in our model at an age of ~ 3 Myr (see the bottom panel of Figure 1). Typically values of M_{disc} are even smaller than $10^{-2} m_*$, so even greater turbulence may be imparted by the ISM. Broadly, for discs older than ~ 3 Myr (as is the case for all those with upper limits on the turbulence) we expect relatively low levels of turbulence, while for younger discs (like DM Tau⁵⁹ and IM Lup⁶¹) turbulence driven by the ISM can also be larger.

We can estimate the distribution of turbulent velocities statistically by directly computing the energy balance in our model. We can write:

$$\dot{E}_{\text{t,disc}} = \epsilon_t \dot{E}_{\text{in}} + \dot{E}_{\text{decay}} + \dot{E}_{\text{acc}}, \quad (20)$$

where we include the accretion term:

$$\dot{E}_{\text{acc}} = -\frac{1}{2}\dot{M}_{\text{acc}}v_{\text{t,disc}}^2, \quad (21)$$

although in practice $|\dot{E}_{\text{acc}}| \ll |\dot{E}_{\text{decay}}|$. Then we can solve the initial value problem, including the mass evolution of the disc as before. In principle, we could then compute the disc evolution fully consistently assuming only the ISM as the driver of internal physics, since we then have α_{SS} or equivalently τ_{acc} . However, in practice, this requires introducing a free parameter ϵ_{t} , which may not be a constant. Strictly, it also means self-consistently evolving the disc outer radius (or disc scale radius), which should viscously expand, such that we can compute the correct v_{in} . This would also be balanced by the contraction due to deposition of low angular momentum material,⁶⁶ resulting in additional (non-turbulent) stellar accretion. For these reasons, self-consistently solving the disc evolution would considerably complicate our model. We therefore leave this to future work. Nonetheless, we can adopt sensible parameters: $\epsilon_{\text{t}} = 1$, $R_{\text{disc}} = 250(m_*/1 M_{\odot})$ au and $H_{\text{disc}} = 0.1R_{\text{disc}}$ with our fixed τ_{acc} to obtain an estimate for the maximal turbulent disc velocity $v_{\text{t,disc}}$ over time. The outcome of this exercise is shown in Figure 4, and discussed in the main article. We find that sufficient turbulent energy is supplied to discs from the ISM to sustain the observed turbulence.

We can also consider the specific case of DM Tau, which is a star of mass $\sim 0.4\text{--}0.5 M_{\odot}$ hosting a disc with a dust cavity and accreting at a rate $\sim 10^{-8} M_{\odot} \text{ yr}^{-1}$.^{116,117} It has a turbulent velocity $v_{\text{t,disc}} \sim 0.25\text{--}0.33 c_{\text{s}}$, or viscous $\alpha_{\text{SS}} \sim 0.1$.⁶ For this disc, a recent and relatively rapid period of accretion would be needed to drive the observed turbulence. Estimating $M_{\text{disc}}/m_* \approx 0.03$,¹¹⁸ this would imply recent accretion from the ISM at a rate $\dot{M}_{\text{BHL}} \gtrsim 2 \times 10^{-8} M_{\odot} \text{ yr}^{-1}$ that

ended in the last $\sim 10^4$ years. This is similar to the current stellar accretion rate,¹¹⁶ suggesting that the majority of the mass of the present day disc could have originated from this putative in-fall event. This scenario is plausible statistically within the context of our model. However, apart from the argument above, there is currently no particular evidence that DM Tau has undergone recent in-fall. This underlines the importance of a systematic search for observational signatures of late stage in-fall events.

Observability of in-fall events: A valid question to ask is the degree to which the model we present in this work predicts more abundant evidence of late-stage in-fall events from the data that is currently available. In fact, growing evidence suggests that a considerable fraction of discs are undergoing some kind of interaction with their environment. For example, a recent scattered light survey of NIR polarimetric imaging for 43 discs in Taurus reported that 16 percent of those discs showed evidence of interaction with ambient material (although this sample is not necessarily representative).³² While inferring observational signatures of late stage in-fall requires full hydrodynamic and radiative transfer simulations,¹¹⁹ we can make a simple estimate for the density of gas we expect to be surrounding discs in our model. For accretion onto a disc from a radius R_{acc} , the maximum free-fall time onto a star of mass m_* is:

$$\tau_{\text{ff,max}} \approx 2 \times 10^3 \left(\frac{R_{\text{acc}}}{250 \text{ au}} \right)^{3/2} \left(\frac{m_*}{1 M_{\odot}} \right)^{-1/2} \text{ years.} \quad (22)$$

Given a BHL accretion rate \dot{M}_{BHL} , we can then estimate the column density of material external to the disc:

$$N_{\text{ext}} \sim 2 \times 10^{19} \epsilon_{\text{geo}}^{-1} \left(\frac{\mu}{2.3} \right)^{-1} \left(\frac{\dot{M}_{\text{BHL}}}{10^{-9} M_{\odot} \text{ yr}^{-1}} \right)^{-1/2} \left(\frac{R_{\text{acc}}}{250 \text{ au}} \right)^{-1/2} \left(\frac{m_*}{1 M_{\odot}} \right)^{-1/2} \text{ cm}^{-2}, \quad (23)$$

where $\epsilon_{\text{geo}} \leq 1$ is a geometric factor accounting for the non-uniform distribution of material and μ is the mean molecular mass.

The typical column density implied by equation 23 is relatively low, such that we would expect that in-fall is often challenging to trace observationally. We may consider the example of CO isotopologues, which are often the brightest tracers used to probe the gas content of protoplanetary discs with ALMA. These isotopologues have a self-shielding column density of $\sim 10^{15} \text{ cm}^{-2}$,^{120,121} and typical abundance relative to molecular hydrogen $\sim 10^{-5}$.¹⁰⁴ As an order of magnitude estimate, we may therefore expect column densities $\lesssim 10^{20} \text{ cm}^{-2}$ to have the CO photodissociated. From equation 23, we plot the N_{ext} distribution over time resulting from the accretion rates in our model in Extended Data Figure 7. We see immediately in-falling CO would be photodissociated for the majority of discs in the age range $\sim 1\text{--}3$ Myr. Interestingly, in this age range, the fraction of discs above the threshold $N_{\text{ext}} = 10^{20} \text{ cm}^{-2}$, approximately the CO self-shielding column, drops from approximately 30 percent to close to 0 percent. Given that this is the range of ages in Taurus, this would be commensurate with the inferred ~ 16 percent of discs with evidence of interaction with the ambient medium from scattered light observations.³² However, the physical column density down to which these observations are sensitive is not clear. While these estimates are approximate, they highlight the importance of deep surveys of the environments surrounding large numbers of discs. Such data could be applied to make statistical inferences about the prevalence of late stage in-fall, testing the theoretical predictions we have made in this work.

Caveats for the ISM accretion rate: In this work, we have considered a simple estimate for the BHL accretion rate. Here we discuss some possible reasons why the rate may deviate from this approximation, and discuss some open questions about the process of capture of interstellar material.

BHL accretion mediated by a disc: The nature of BHL accretion has a long history of testing with numerical experiments. In a supersonic, uniform medium, these broadly validate the analytic estimate for the BHL accretion rate within a factor of order unity.^{34, 122–126} In a turbulent medium, the instantaneous accretion rate may be limited by the local vorticity instead of the velocity.⁴³ In this case there may be a substantial reduction in the accretion rate, but only when the Mach number is low (i.e. $\Delta v \sim c_s$), which is rarely the case in our numerical calculations. In a magnetised medium, the BHL accretion rate may also be reduced by a factor ~ 2 , although this is dependent on the ratio of magnetic to thermal pressure.^{75, 76} Overall, we expect our simple estimates to yield a reasonable approximation for the mass accretion rate.

A further pertinent question is what we expect the appearance of the resultant disc to be. As previously discussed, when accreting material with with a high vorticity, the resultant disc outer radius can be of order the BHL radius – see, for example, Figure 3 of Krumholz et al. (2006).⁴³ What is more uncertain is what should be the structure of a disc if the angular momentum of the accreted material is not aligned with the existing material. Naively, such randomised angular momentum could result in ‘puffed up’ discs. By contrast, at least the mm-dust component of discs is frequently observed to be extremely flat.^{5, 62, 127–129} However, mm-dust is also commonly

more centrally concentrated than the gaseous disc by a factor ~ 2.5 .^{48, 130, 131} Since dust radial drift, growth and vertical settling should occur simultaneously, it is not clear how accretion of turbulent gas in the outer disc should be reflected in the dust distribution. This represents an important topic for future study.

Cloudlet capture: Another possible avenue for the capture of interstellar gas is the capture of small cloudlets via tidal energy dissipation. During the close passage between a star and a cloud, the orbital energy may be dissipated by non-radial oscillations within the cloud, analogous to the formation of tight binaries in globular clusters,^{132, 133} in a process that remains similar across a range of internal density profiles.¹³⁴ Capture requires a periastron a_p during an encounter between a cloud with radius R_{cloud} and mass M_{cloud} and star with mass m_* such that:

$$a_p \lesssim a_{\text{capt}} \approx R_{\text{cloud}} \left[\frac{Gm_*}{R_{\text{cloud}}v_\infty^2} q_{\text{cloud}}^{-1} (1 + q_{\text{cloud}}) \right]^{1/6}. \quad (24)$$

Here $q_{\text{cloud}} = M_{\text{cloud}}/m_*$, and v_∞ is the relative velocity between star and cloud at infinite separation.

Then if $a_{\text{capt}} > R_{\text{cloud}}$, the cross section is:

$$\sigma_{\text{capt}} \approx \frac{2\pi Gm_*(1 + q_{\text{cloud}})(a_{\text{capt}} - R_{\text{cloud}})}{v_\infty^2}. \quad (25)$$

We have made the conservative assumption that only gravitationally focused encounters may result in capture. We exclude encounters for which the star passes through the cloud, which would result in BHL accretion, although even in this case tidal effects may be relevant for a dense ISM.

The cloud must be compact enough to be captured fully by the star. Therefore the total rate

of capture for a cloud of radius R_{cloud} is:

$$\Gamma_{\text{capt}}(R_{\text{cloud}}|\rho_{\text{cloud}}, \sigma_v) = \int_0^{v_{\text{BHL}}} n_{\text{clouds}}(R_{\text{cloud}}) \sigma_{\text{capt}} \tilde{v} g_3(\tilde{v}|\sigma_v) d\tilde{v}, \quad (26)$$

where

$$g_{N_D}(\Delta v|\sigma_v) = \frac{2\Delta v^{N_D-1}}{\Gamma(N_D/2)} \left(\frac{1}{4\sigma_v^2}\right)^{N_D/2} \exp\left(\frac{-\Delta v^2}{4\sigma_v^2}\right) \quad (27)$$

is the Maxwell-Boltzmann distributions in N_D dimensions. We have cast equation 26 in terms of the cloud density $\rho_{\text{cloud}} = 3M_{\text{cloud}}/4\pi R_{\text{cloud}}^3$. If large scale turbulence dominates density fluctuations, we can estimate that a typical cloud density will be $\rho_{\text{cloud}} \sim \rho_{\text{gas}}$. We have introduced $n_{\text{clouds}} = 1/(2R_{\text{cloud}})^3$, where $2R_{\text{cloud}}$ is the wavelength of the turbulent oscillations in the ISM that produce a cloud of radius R_{cloud} . Finally, we have defined the BHL velocity v_{BHL} , which is the velocity that yields a particular $R_{\text{BHL}} = R_{\text{cloud}}$ when substituted into equation 6. The overall accretion rate is then $\dot{M}_{\text{capt}} = \Gamma_{\text{capt}} M_{\text{cloud}}$.

In Extended Data Figure 8, we show the results of these calculations for a solar mass star in an ISM of density $\rho_{\text{gas}} = 100 M_{\odot} \text{pc}^{-3}$. We find that capture rates are typically maximised for cloud sizes $R_{\text{cloud}} \sim 0.1-1R_{\text{BHL}}$. Assuming $R_{\text{acc}} = R_{\text{BHL}}$ and substituting in $\Delta v_{\text{gas}} = 1 \text{ km s}^{-1}$ for a solar mass star into equation 9 yields $\dot{M}_{\text{BHL}} \approx 2.4 \times 10^{-8} M_{\odot} \text{yr}^{-1}$. Inferring the comparable cloud capture accretion rate from Extended Data Figure 8 yields a very similar rate. In general, we expect that tidal cloud capture may play a significant role in disc assembly, alongside BHL accretion. This may increase the rate of interstellar gas capture by a factor of order unity, and may be the subject of future numerical experiment.

Face-on accretion: A third mechanism for ISM accretion is face-on disc accretion, where an

existing disc produces a large physical cross-section.^{66,88} In this case, the ram pressure between a pre-existing disc and the ISM mediates the accretion process. Face-on accretion may be significant when a star moves through a relatively high velocity medium. In this case, the disc shrinks as a result of deposition of low angular momentum material onto the disc surface.⁶⁶ There is no steady state for this process unless material can be constantly replenished. This replenishment of outer disc material may be viscous, but then the quantity of material accreted is limited by the initial disc mass. Replenishment via BHL or cloud capture would keep the disc at a radius $R_{\text{disc}} \sim R_{\text{BHL}}$, and would therefore result in a similar accretion rate to BHL accretion.⁸⁸ However, this may significantly enhance accretion rates when the BHL radius decreases; then $R_{\text{disc}} > R_{\text{BHL}}$. Face-on accretion would then temporarily dominate the overall rate, shrinking the disc to maintain a balance between shrinkage and replenishment. Overall, we may expect some moderate enhancement to the rate of capture and stellar accretion during short phases, although this would not be expected to greatly change the overall disc evolution.

Consequences of ISM regulated discs: Our results strongly suggest that disc properties are regulated by a continuous process of ISM accretion. This would have numerous consequences, many of which should be investigated in future work. We briefly summarise some examples as follows:

- *Disc sub-structures:* A diverse range of substructures have been observed in protoplanetary discs.⁴⁸ We have demonstrated that the disc is undergoing constant perturbation by in-falling material. We would therefore expect some discs to exhibit structure due to this process.¹⁷ For example, by accreting gas from the ISM with a misaligned angular momentum vector

we expect disc warping,¹³⁵ which may also produce observable shadows.^{119,136} Both external structures and disc warping are evident in some discs,⁹ and it seems probable that they originate from late stage in-fall at least in some instances.

- *Accretion outbursts and short accretion times:* FU Orionis events are short accretion bursts that last ~ 100 years,¹³⁷ named for the archetypal example.^{138,139} In-fall events are among the earliest explanations for these events. There remain several other possible mechanisms such as stellar encounters^{140,141} and thermal instability,^{142–144} although extended nebulosity surrounding several stars undergoing outburst strongly supports the role of in-fall in at least some cases.^{145,146} Outbursting star-disc systems may be more broadly categorised as a subset of systems with short accretion time-scales.^{42,44} Among such discs, a lifetime problem appears particularly pronounced for discs around some Herbig stars.¹⁴⁷ The assumptions of our model mean that we cannot directly explain these short accretion time-scales; we *impose* this time-scale for our model. However, given a fixed time-scale τ_{acc} , discs with short τ_{acc} may be episodically replenished in our model. Thus, to a degree the inferred accretion time-scale is decoupled from the expected frequency of observed discs, which no longer needs to be $\sim \tau_{\text{acc}}/\tau_{\text{disc}}$, for disc age τ_{disc} . Instead, the frequency of discs with a given τ_{acc} would be dictated by the frequency of in-fall events that lead to rapid mass gain. Indeed, in our model a small number of discs with very short accretion time-scales (~ 0.01 Myr) are retained for ~ 3 Myr (Extended Data Figure 4). Whether the in-fall itself can also produce a short-lived dip in the accretion time-scale (i.e. an outburst) depends on the turbulence imparted onto the disc, and may depend on the rate or physics of interstellar gas accretion (as discussed

above).

- *Long-lived discs:* Stochastic replenishment of discs represents a simple explanation for so-called ‘Peter Pan’ discs, which are (low mass) stars that are tens of Myr old but still exhibit a gas-rich accretion disc.^{108, 148, 149} It is not clear if Peter Pan discs are exclusively around low mass stars, or whether finding discs around M dwarf stars is just down to sampling of the mass function. Speculatively, this phenomenon may be related to the fact that individual massive discs appear across a number of regions of different ages, even where the majority of discs have been depleted.¹⁵⁰ Late stage in-fall seems a viable way to explain some of these long-lived discs. This further motivates deep observational programs to characterise the super-disc scale gas surrounding protoplanetary discs.
- *Planet properties:* Possibly the most exciting consequence of protoplanetary discs that are regulated by BHL accretion would be the potential consequences for planets. Multiple studies have shown that mature planet properties are dependent on stellar kinematics.^{151, 152} Some of these differences could be related to covariance with stellar properties, such as age and metallicity.¹⁵³ However, it is not clear that all correlations can be explained by stellar properties alone.^{154–156} If discs are constantly replenished by the ISM, stars that form at high velocity relative to the local rest frame should accrete less mass from the ISM after the dispersal of their formation cloud. This represents a direct theoretical link between planet formation and stellar kinematics.

1. Haisch, K. E., Jr., Lada, E. A. & Lada, C. J. Disk Frequencies and Lifetimes in Young Clusters. *Astrophys. J. Let.* **553**, L153–L156 (2001).
2. Hartlep, T. & Cuzzi, J. N. Cascade Model for Planetesimal Formation by Turbulent Clustering. *Astrophys. J.* **892**, 120 (2020).
3. Lega, E. *et al.* Migration of Jupiter mass planets in discs with laminar accretion flows. *Astron. Astrophys.* **658**, A32 (2022).
4. Wafflard-Fernandez, G. & Lesur, G. Planet-disk-wind interaction: The magnetized fate of protoplanets. *Astron. Astrophys.* **677**, A70 (2023).
5. Villenave, M. *et al.* Observations of edge-on protoplanetary disks with ALMA. I. Results from continuum data. *Astron. Astrophys.* **642**, A164 (2020).
6. Flaherty, K. *et al.* Measuring Turbulent Motion in Planet-forming Disks with ALMA: A Detection around DM Tau and Nondetections around MWC 480 and V4046 Sgr. *Astrophys. J.* **895**, 109 (2020).
7. Rosotti, G. P. Empirical constraints on turbulence in proto-planetary discs. *New A Rev.* **96**, 101674 (2023).
8. Fukagawa, M. *et al.* Spiral Structure in the Circumstellar Disk around AB Aurigae. *Astrophys. J. Let.* **605**, L53–L56 (2004).
9. Walsh, C., Daley, C., Facchini, S. & Juhász, A. CO emission tracing a warp or radial flow within $\lesssim 100$ au in the HD 100546 protoplanetary disk. *Astron. Astrophys.* **607**, A114 (2017).

10. Gupta, A. *et al.* TIPSYP: Trajectory of Infalling Particles in Streamers around Young stars. Dynamical analysis of the streamers around S CrA and HL Tau. *Astron. Astrophys.* **683**, A133 (2024).
11. Winter, A. J. & Haworth, T. J. The external photoevaporation of planet-forming discs. *European Physical Journal Plus* **137**, 1132 (2022).
12. Cuello, N., Ménard, F. & Price, D. J. Close encounters: How stellar flybys shape planet-forming discs. *European Physical Journal Plus* **138**, 11 (2023).
13. Huang, J. *et al.* Molecules with ALMA at Planet-forming Scales (MAPS). XIX. Spiral Arms, a Tail, and Diffuse Structures Traced by CO around the GM Aur Disk. *Astrophys. J. Supp.* **257**, 19 (2021).
14. Garufi, A. *et al.* Disks Around T Tauri Stars with SPHERE (DARTTS-S). II. Twenty-one new polarimetric images of young stellar disks. *Astron. Astrophys.* **633**, A82 (2020).
15. Benisty, M. *et al.* Optical and Near-infrared View of Planet-forming Disks and Protoplanets. In Inutsuka, S., Aikawa, Y., Muto, T., Tomida, K. & Tamura, M. (eds.) *Protostars and Planets VII*, vol. 534 of *Astronomical Society of the Pacific Conference Series*, 605 (2023). 2203. 09991.
16. Dullemond, C. P. *et al.* Cloudlet capture by transitional disk and FU Orionis stars. *Astron. Astrophys.* **628**, A20 (2019).
17. Kuffmeier, M., Goicovic, F. G. & Dullemond, C. P. Late encounter events as source of disks and spiral structures. Forming second generation disks. *Astron. Astrophys.* **633**, A3 (2020).

18. Hanawa, T., Garufi, A., Podio, L., Codella, C. & Segura-Cox, D. Cloudlet capture model for the accretion streamer onto the disc of DG Tau. *Mon. Not. R. Astron. Soc.* **528**, 6581–6592 (2024).
19. Huang, J., Bergin, E. A., Bae, J., Benisty, M. & Andrews, S. M. Molecular Mapping of DR Tau’s Protoplanetary Disk, Envelope, Outflow, and Large-scale Spiral Arm. *Astrophys. J.* **943**, 107 (2023).
20. Boccaletti, A. *et al.* Possible evidence of ongoing planet formation in AB Aurigae. A showcase of the SPHERE/ALMA synergy. *Astron. Astrophys.* **637**, L5 (2020).
21. Gupta, A. *et al.* Reflections on nebulae around young stars. A systematic search for late-stage infall of material onto Class II disks. *Astron. Astrophys.* **670**, L8 (2023).
22. Pérez, S. *et al.* Resolving the FU Orionis System with ALMA: Interacting Twin Disks? *Astrophys. J.* **889**, 59 (2020).
23. Hales, A. S. *et al.* ALMA Observations of Young Eruptive Stars: Continuum Disk Sizes and Molecular Outflows. *Astrophys. J.* **900**, 7 (2020).
24. Dong, R. *et al.* A likely flyby of binary protostar Z CMa caught in action. *Nature Astronomy* **6**, 331–338 (2022).
25. Ginski, C. *et al.* Disk Evolution Study Through Imaging of Nearby Young Stars (DESTINYs): Late Infall Causing Disk Misalignment and Dynamic Structures in SU Aur. *Astrophys. J. Let.* **908**, L25 (2021).

26. Jørgensen, J. K. *et al.* PROSAC: a submillimeter array survey of low-mass protostars. II. The mass evolution of envelopes, disks, and stars from the Class 0 through I stages. *Astron. Astrophys.* **507**, 861–879 (2009).
27. Maury, A. J. *et al.* Characterizing young protostellar disks with the CALYPSO IRAM-PdBI survey: large Class 0 disks are rare. *Astron. Astrophys.* **621**, A76 (2019).
28. Codella, C. *et al.* Faust xii. accretion streamers and jets in the vla 1623–2417 protocluster (2024). 2402.10258.
29. Nakajima, T. & Golimowski, D. A. Coronagraphic Imaging of Pre-Main-Sequence Stars: Remnant Envelopes of Star Formation Seen in Reflection. *Astron. J.* **109**, 1181 (1995).
30. Grady, C. A. *et al.* Hubble Space Telescope Space Telescope Imaging Spectrograph Coronagraphic Imaging of the Herbig AE Star AB Aurigae. *Astrophys. J. Let.* **523**, L151–L154 (1999).
31. Mesa, D. *et al.* Signs of late infall and possible planet formation around DR Tau using VLT/SPHERE and LBTI/LMIRCam. *Astron. Astrophys.* **658**, A63 (2022).
32. Garufi, A. *et al.* The SPHERE view of the Taurus star-forming region. *arXiv e-prints* arXiv:2403.02158 (2024).
33. Bondi, H. On spherically symmetrical accretion. *Mon. Not. R. Astron. Soc.* **112**, 195 (1952).
34. Edgar, R. A review of Bondi-Hoyle-Lyttleton accretion. *New A Rev.* **48**, 843–859 (2004).

35. Padoan, P., Kritsuk, A., Norman, M. L. & Nordlund, Å. A Solution to the Pre-Main-Sequence Accretion Problem. *Astrophys. J. Let.* **622**, L61–L64 (2005).
36. Throop, H. B. & Bally, J. Tail-End Bondi-Hoyle Accretion in Young Star Clusters: Implications for Disks, Planets, and Stars. *Astron. J.* **135**, 2380–2397 (2008).
37. Klessen, R. S. & Hennebelle, P. Accretion-driven turbulence as universal process: galaxies, molecular clouds, and protostellar disks. *Astron. Astrophys.* **520**, A17 (2010).
38. Bond, J. R., Cole, S., Efstathiou, G. & Kaiser, N. Excursion Set Mass Functions for Hierarchical Gaussian Fluctuations. *Astrophys. J.* **379**, 440 (1991).
39. Hopkins, P. F. An excursion-set model for the structure of giant molecular clouds and the interstellar medium. *Mon. Not. R. Astron. Soc.* **423**, 2016–2036 (2012).
40. Girichidis, P., Konstandin, L., Whitworth, A. P. & Klessen, R. S. On the Evolution of the Density Probability Density Function in Strongly Self-gravitating Systems. *Astrophys. J.* **781**, 91 (2014).
41. Matzner, C. D. & McKee, C. F. Efficiencies of Low-Mass Star and Star Cluster Formation. *Astrophys. J.* **545**, 364–378 (2000).
42. Manara, C. F. *et al.* Demographics of Young Stars and their Protoplanetary Disks: Lessons Learned on Disk Evolution and its Connection to Planet Formation. In Inutsuka, S., Aikawa, Y., Muto, T., Tomida, K. & Tamura, M. (eds.) *Astronomical Society of the Pacific Conference Series*, vol. 534 of *Astronomical Society of the Pacific Conference Series*, 539 (2023). 2203.09930.

43. Krumholz, M. R., McKee, C. F. & Klein, R. I. Bondi-Hoyle Accretion in a Turbulent Medium. *Astrophys. J.* **638**, 369–381 (2006).
44. Almendros-Abad, V. *et al.* Evolution of the relation between the mass accretion rate and the stellar and disk mass from brown dwarfs to stars (2024). 2402.10523.
45. Testi, L. *et al.* Brown dwarf disks with ALMA: Evidence for truncated dust disks in Ophiuchus. *Astron. Astrophys.* **593**, A111 (2016).
46. Cieza, L. A. *et al.* The Ophiuchus DIsc Survey Employing ALMA (ODISEA) - I: project description and continuum images at 28 au resolution. *Mon. Not. R. Astron. Soc.* **482**, 698–714 (2019).
47. Testi, L. *et al.* The protoplanetary disk population in the ρ -Ophiuchi region L1688 and the time evolution of Class II YSOs. *Astron. Astrophys.* **663**, A98 (2022).
48. Andrews, S. M. Observations of Protoplanetary Disk Structures. *Annu. Rev. Astron. Astrophys.* **58**, 483–528 (2020).
49. Sanchis, E. *et al.* Measuring the ratio of the gas and dust emission radii of protoplanetary disks in the Lupus star-forming region. *Astron. Astrophys.* **649**, A19 (2021).
50. Garufi, A. *et al.* ALMA chemical survey of disk-outflow sources in Taurus (ALMA-DOT). VI. Accretion shocks in the disk of DG Tau and HL Tau. *Astron. Astrophys.* **658**, A104 (2022).

51. Shakura, N. I. & Sunyaev, R. A. Black holes in binary systems. Observational appearance. *Astron. Astrophys.* **24**, 337–355 (1973).
52. Cuzzi, J. N., Hogan, R. C., Paque, J. M. & Dobrovolskis, A. R. Size-selective Concentration of Chondrules and Other Small Particles in Protoplanetary Nebula Turbulence. *Astrophys. J.* **546**, 496–508 (2001).
53. Sokal, K. R. *et al.* Characterizing TW Hydra. *Astrophys. J.* **853**, 120 (2018).
54. Flaherty, K. M. *et al.* Turbulence in the TW Hya Disk. *Astrophys. J.* **856**, 117 (2018).
55. van den Ancker, M. E., de Winter, D. & Tjin A Djie, H. R. E. HIPPARCOS photometry of Herbig Ae/Be stars. *Astron. Astrophys.* **330**, 145–154 (1998).
56. Flaherty, K. M. *et al.* A Three-dimensional View of Turbulence: Constraints on Turbulent Motions in the HD 163296 Protoplanetary Disk Using DCO⁺. *Astrophys. J.* **843**, 150 (2017).
57. Simon, M., Dutrey, A. & Guilloteau, S. Dynamical Masses of T Tauri Stars and Calibration of Pre-Main-Sequence Evolution. *Astrophys. J.* **545**, 1034–1043 (2000).
58. Torres, C. A. O., Quast, G. R., Melo, C. H. F. & Sterzik, M. F. Young Nearby Loose Associations. In Reipurth, B. (ed.) *Handbook of Star Forming Regions, Volume II*, vol. 5, 757 (2008).
59. Zhang, K., Schwarz, K. R. & Bergin, E. A. Rapid Evolution of Volatile CO from the Protostellar Disk Stage to the Protoplanetary Disk Stage. *Astrophys. J. Let.* **891**, L17 (2020).

60. Paneque-Carreño, T. *et al.* High turbulence in the IM Lup protoplanetary disk. Direct observational constraints from CN and C₂H emission. *Astron. Astrophys.* **684**, A174 (2024).
61. Mawet, D. *et al.* Direct imaging of extra-solar planets in star forming regions. Lessons learned from a false positive around IM Lupi. *Astron. Astrophys.* **544**, A131 (2012).
62. Villenave, M. *et al.* A Highly Settled Disk around Oph163131. *Astrophys. J.* **930**, 11 (2022).
63. Villenave, M. *et al.* Modest Dust Settling in the IRAS04302+2247 Class I Protoplanetary Disk. *Astrophys. J.* **946**, 70 (2023).
64. Lin, Z.-Y. D. *et al.* Early Planet Formation in Embedded Disks (eDisk). II. Limited Dust Settling and Prominent Snow Surfaces in the Edge-on Class I Disk IRAS 04302+2247. *Astrophys. J.* **951**, 9 (2023).
65. Hartmann, L., Calvet, N., Gullbring, E. & D'Alessio, P. Accretion and the Evolution of T Tauri Disks. *Astrophys. J.* **495**, 385–400 (1998).
66. Wijnens, T. P. G., Pols, O. R., Pelupessy, F. I. & Portegies Zwart, S. Characterising face-on accretion onto and the subsequent contraction of protoplanetary discs. *Astron. Astrophys.* **602**, A52 (2017).
67. Lesur, G. *et al.* Hydro-, Magnetohydro-, and Dust-Gas Dynamics of Protoplanetary Disks. In Inutsuka, S., Aikawa, Y., Muto, T., Tomida, K. & Tamura, M. (eds.) *Protostars and Planets VII*, vol. 534 of *Astronomical Society of the Pacific Conference Series*, 465 (2023).

68. Goldsmith, P. F. *et al.* Large-Scale Structure of the Molecular Gas in Taurus Revealed by High Linear Dynamic Range Spectral Line Mapping. *Astrophys. J.* **680**, 428–445 (2008).
69. Colman, T. *et al.* The signature of large-scale turbulence driving on the structure of the interstellar medium. *Mon. Not. R. Astron. Soc.* **514**, 3670–3684 (2022).
70. Nusser, A. & Silk, J. Regulation of star formation by large-scale gravitoturbulence. *Mon. Not. R. Astron. Soc.* **509**, 2979–2993 (2022).
71. Vazquez-Semadeni, E. Hierarchical Structure in Nearly Pressureless Flows as a Consequence of Self-similar Statistics. *Astrophys. J.* **423**, 681 (1994).
72. Burgers, J. In Von Mises, R. & Von Kármán, T. (eds.) *A Mathematical Model Illustrating the Theory of Turbulence*, vol. 1 of *Advances in Applied Mechanics*, 171–199 (Elsevier, 1948). URL <https://www.sciencedirect.com/science/article/pii/S0065215608701005>.
73. Begelman, M. C. & Shlosman, I. Angular Momentum Transfer and Lack of Fragmentation in Self-Gravitating Accretion Flows. *Astrophys. J. Let.* **702**, L5–L8 (2009).
74. Jeans, J. H. The Stability of a Spherical Nebula. *Philosophical Transactions of the Royal Society of London Series A* **199**, 1–53 (1902).
75. Lee, A. T., Cunningham, A. J., McKee, C. F. & Klein, R. I. Bondi-Hoyle Accretion in an Isothermal Magnetized Plasma. *Astrophys. J.* **783**, 50 (2014).

76. Burleigh, K. J., McKee, C. F., Cunningham, A. J., Lee, A. T. & Klein, R. I. Bondi-Hoyle accretion in a turbulent, magnetized medium. *Mon. Not. R. Astron. Soc.* **468**, 717–727 (2017).
77. Pan, L. & Scannapieco, E. Mixing in Supersonic Turbulence. *Astrophys. J.* **721**, 1765–1782 (2010).
78. Pfalzner, S., Dehghani, S. & Michel, A. Most Planets Might Have More than 5 Myr of Time to Form. *Astrophys. J. Let.* **939**, L10 (2022).
79. Joncour, I., Duchêne, G., Moraux, E. & Motte, F. Multiplicity and clustering in Taurus star forming region. II. From ultra-wide pairs to dense NESTs. *Astron. Astrophys.* **620**, A27 (2018).
80. Preibisch, T., Brown, A. G. A., Bridges, T., Guenther, E. & Zinnecker, H. Exploring the Full Stellar Population of the Upper Scorpius OB Association. *Astron. J.* **124**, 404–416 (2002).
81. Miret-Roig, N. *et al.* The star formation history of Upper Scorpius and Ophiuchus. A 7D picture: positions, kinematics, and dynamical traceback ages. *Astron. Astrophys.* **667**, A163 (2022).
82. Hillenbrand, L. A. & Hartmann, L. W. A Preliminary Study of the Orion Nebula Cluster Structure and Dynamics. *Astrophys. J.* **492**, 540–553 (1998).
83. Reid, M. J. *et al.* Trigonometric Parallaxes of Massive Star-Forming Regions. VI. Galactic Structure, Fundamental Parameters, and Noncircular Motions. *Astrophys. J.* **700**, 137–148 (2009).

84. Zucker, C. *et al.* Star formation near the Sun is driven by expansion of the Local Bubble. *Nature* **601**, 334–337 (2022).
85. Hoyle, F. On the Fragmentation of Gas Clouds Into Galaxies and Stars. *Astrophys. J.* **118**, 513 (1953).
86. Vázquez-Semadeni, E., Palau, A., Ballesteros-Paredes, J., Gómez, G. C. & Zamora-Avilés, M. Global hierarchical collapse in molecular clouds. Towards a comprehensive scenario. *Mon. Not. R. Astron. Soc.* **490**, 3061–3097 (2019).
87. Shima, E., Matsuda, T., Takeda, H. & Sawada, K. Hydrodynamic calculations of axisymmetric accretion flow. *Mon. Not. R. Astron. Soc.* **217**, 367–386 (1985).
88. Moeckel, N. & Throop, H. B. Bondi-Hoyle-Lyttleton Accretion Onto a Protoplanetary Disk. *Astrophys. J.* **707**, 268–277 (2009).
89. Lynden-Bell, D. & Pringle, J. E. The evolution of viscous discs and the origin of the nebular variables. *Mon. Not. R. Astron. Soc.* **168**, 603–637 (1974).
90. Tabone, B., Rosotti, G. P., Cridland, A. J., Armitage, P. J. & Lodato, G. Secular evolution of MHD wind-driven discs: analytical solutions in the expanded α -framework. *Mon. Not. R. Astron. Soc.* **512**, 2290–2309 (2022).
91. Tobin, J. J. *et al.* The VLA/ALMA Nascent Disk and Multiplicity (VANDAM) Survey of Orion Protostars. IV. Unveiling the Embedded Intermediate-Mass Protostar and Disk within OMC2-FIR3/HOPS-370. *Astrophys. J.* **905**, 162 (2020).

92. Soderblom, D. R., Hillenbrand, L. A., Jeffries, R. D., Mamajek, E. E. & Naylor, T. Ages of Young Stars. In Beuther, H., Klessen, R. S., Dullemond, C. P. & Henning, T. (eds.) *Protostars and Planets VI*, 219–241 (2014). 1311.7024.
93. Luhman, K. L. & Rieke, G. H. Low-Mass Star Formation and the Initial Mass Function in the ρ Ophiuchi Cloud Core. *Astrophys. J.* **525**, 440–465 (1999).
94. Krolkowski, D. M., Kraus, A. L. & Rizzuto, A. C. Gaia EDR3 Reveals the Substructure and Complicated Star Formation History of the Greater Taurus-Auriga Star-forming Complex. *Astron. J.* **162**, 110 (2021).
95. Galli, P. A. B. *et al.* Lupus DANCe. Census of stars and 6D structure with Gaia-DR2 data. *Astron. Astrophys.* **643**, A148 (2020).
96. Galli, P. A. B. *et al.* Chamaeleon DANCe. Revisiting the stellar populations of Chamaeleon I and Chamaeleon II with Gaia-DR2 data. *Astron. Astrophys.* **646**, A46 (2021).
97. Luhman, K. L. The Stellar Population of the Chamaeleon I Star-forming Region. *Astrophys. J. Supp.* **173**, 104–136 (2007).
98. Pecaut, M. J. & Mamajek, E. E. The star formation history and accretion-disc fraction among the K-type members of the Scorpius-Centaurus OB association. *Mon. Not. R. Astron. Soc.* **461**, 794–815 (2016).
99. Luhman, K. L. & Esplin, T. L. Refining the Census of the Upper Scorpius Association with Gaia. *Astron. J.* **160**, 44 (2020).

100. Scott, D. W. *Multivariate Density Estimation* (1992).
101. Williams, J. P. *et al.* The Ophiuchus DIsk Survey Employing ALMA (ODISEA): Disk Dust Mass Distributions across Protostellar Evolutionary Classes. *Astrophys. J. Let.* **875**, L9 (2019).
102. Cazzoletti, P. *et al.* ALMA survey of Class II protoplanetary disks in Corona Australis: a young region with low disk masses. *Astron. Astrophys.* **626**, A11 (2019).
103. Rosotti, G. P. *et al.* The time evolution of dusty protoplanetary disc radii: observed and physical radii differ. *Mon. Not. R. Astron. Soc.* **486**, 4829–4844 (2019).
104. Trapman, L., Rosotti, G., Zhang, K. & Tabone, B. How Large Is a Disk-What Do Protoplanetary Disk Gas Sizes Really Mean? *Astrophys. J.* **954**, 41 (2023).
105. Ribas, Á., Bouy, H. & Merín, B. Protoplanetary disk lifetimes vs. stellar mass and possible implications for giant planet populations. *Astron. Astrophys.* **576**, A52 (2015).
106. Michel, A., van der Marel, N. & Matthews, B. C. Bridging the Gap between Protoplanetary and Debris Disks: Separate Evolution of Millimeter and Micrometer-sized Dust. *Astrophys. J.* **921**, 72 (2021).
107. Kraus, A. L., Ireland, M. J., Hillenbrand, L. A. & Martinache, F. The Role of Multiplicity in Disk Evolution and Planet Formation. *Astrophys. J.* **745**, 19 (2012).
108. Galli, P. A. B. *et al.* χ^1 Fornacis cluster DANCe. Census of stars, structure, and kinematics of the cluster with Gaia-EDR3. *Astron. Astrophys.* **654**, A122 (2021).

109. Clarke, C. J., Gendrin, A. & Sotomayor, M. The dispersal of circumstellar discs: the role of the ultraviolet switch. *Mon. Not. R. Astron. Soc.* **328**, 485–491 (2001).
110. Alexander, R. D., Clarke, C. J. & Pringle, J. E. Photoevaporation of protoplanetary discs - I. Hydrodynamic models. *Mon. Not. R. Astron. Soc.* **369**, 216–228 (2006).
111. Gorti, U. & Hollenbach, D. Photoevaporation of Circumstellar Disks By Far-Ultraviolet, Extreme-Ultraviolet and X-Ray Radiation from the Central Star. *Astrophys. J.* **690**, 1539–1552 (2009).
112. Owen, J. E., Ercolano, B., Clarke, C. J. & Alexander, R. D. Radiation-hydrodynamic models of X-ray and EUV photoevaporating protoplanetary discs. *Mon. Not. R. Astron. Soc.* **401**, 1415–1428 (2010).
113. Picogna, G., Ercolano, B., Owen, J. E. & Weber, M. L. The dispersal of protoplanetary discs - I. A new generation of X-ray photoevaporation models. *Mon. Not. R. Astron. Soc.* **487**, 691–701 (2019).
114. Flaherty, K. M. *et al.* Weak Turbulence in the HD 163296 Protoplanetary Disk Revealed by ALMA CO Observations. *Astrophys. J.* **813**, 99 (2015).
115. Teague, R. *et al.* Temperature, Mass, and Turbulence: A Spatially Resolved Multiband Non-LTE Analysis of CS in TW Hya. *Astrophys. J.* **864**, 133 (2018).
116. Manara, C. F. *et al.* Gas content of transitional disks: a VLT/X-Shooter study of accretion and winds. *Astron. Astrophys.* **568**, A18 (2014).

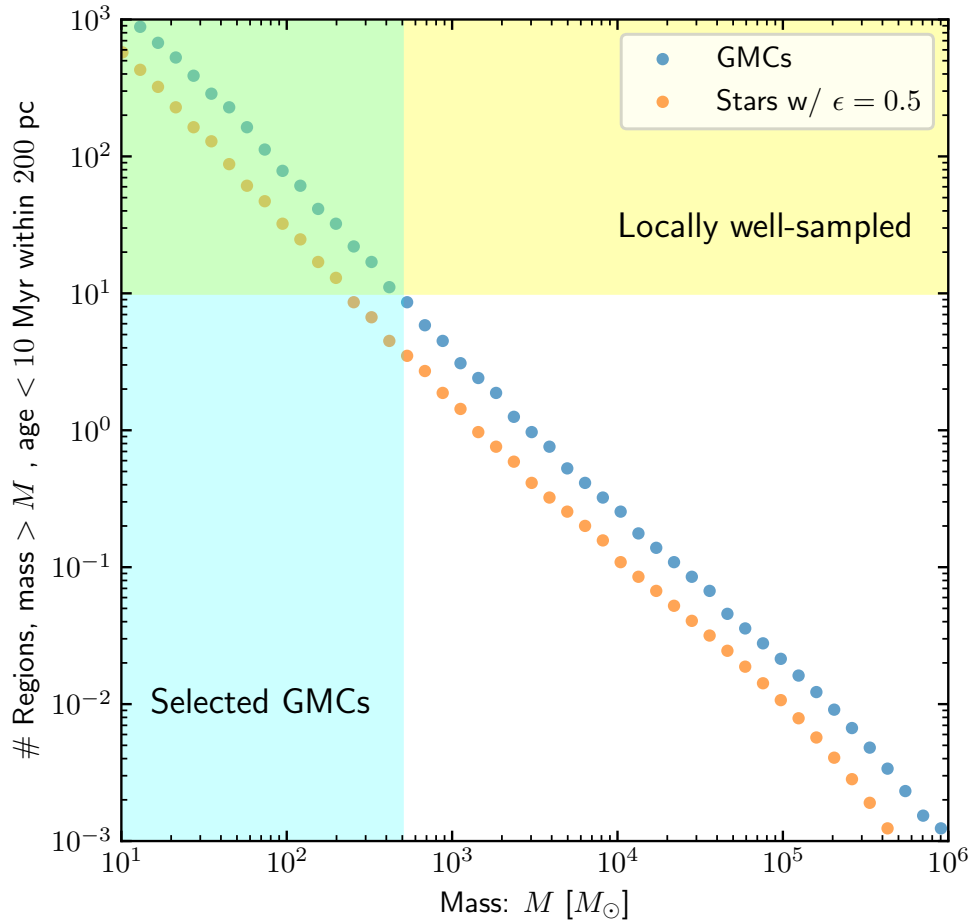
117. Francis, L. & van der Marel, N. Dust-depleted Inner Disks in a Large Sample of Transition Disks through Long-baseline ALMA Observations. *Astrophys. J.* **892**, 111 (2020).
118. Andrews, S. M., Rosenfeld, K. A., Kraus, A. L. & Wilner, D. J. The Mass Dependence between Protoplanetary Disks and their Stellar Hosts. *Astrophys. J.* **771**, 129 (2013).
119. Krieger, A. *et al.* Feasibility of detecting shadows in disks induced by infall. *arXiv e-prints* arXiv:2403.08388 (2024).
120. van Dishoeck, E. F. & Black, J. H. The Photodissociation and Chemistry of Interstellar CO. *Astrophys. J.* **334**, 771 (1988).
121. Visser, R., van Dishoeck, E. F. & Black, J. H. The photodissociation and chemistry of CO isotopologues: applications to interstellar clouds and circumstellar disks. *Astron. Astrophys.* **503**, 323–343 (2009).
122. Hunt, R. A fluid dynamical study of the accretion process. *Mon. Not. R. Astron. Soc.* **154**, 141 (1971).
123. Hunt, R. Accretion of gas having specific heat ratio $3/3$ by a moving gravitating body. *Mon. Not. R. Astron. Soc.* **188**, 83–91 (1979).
124. Ruffert, M. Three-dimensional hydrodynamic Bondi-Hoyle accretion. III. Mach 0.6, 1.4 and 10; $\gamma=5/3$. *A&AS* **106**, 505–522 (1994).
125. Ruffert, M. Three-dimensional hydrodynamic Bondi-Hoyle accretion. V. Specific heat ratio 1.01, nearly isothermal flow. *Astron. Astrophys.* **311**, 817–832 (1996).

126. El Mellah, I. & Casse, F. Numerical simulations of axisymmetric hydrodynamical Bondi-Hoyle accretion on to a compact object. *Mon. Not. R. Astron. Soc.* **454**, 2657–2667 (2015).
127. Duchêne, G., Ménard, F., Stapelfeldt, K. & Duvert, G. A layered edge-on circumstellar disk around HK Tau B. *Astron. Astrophys.* **400**, 559–565 (2003).
128. Pinte, C., Fouchet, L., Ménard, F., Gonzalez, J. F. & Duchêne, G. On the stratified dust distribution of the GG Tauri circumbinary ring. *Astron. Astrophys.* **469**, 963–971 (2007).
129. Pinte, C. *et al.* Dust and Gas in the Disk of HL Tauri: Surface Density, Dust Settling, and Dust-to-gas Ratio. *Astrophys. J.* **816**, 25 (2016).
130. Ansdell, M. *et al.* ALMA Survey of Lupus Protoplanetary Disks. II. Gas Disk Radii. *Astrophys. J.* **859**, 21 (2018).
131. Facchini, S. *et al.* High gas-to-dust size ratio indicating efficient radial drift in the mm-faint CX Tauri disk. *Astron. Astrophys.* **626**, L2 (2019).
132. Robe, H. Les oscillations non radiales des polytropes. *Annales d’Astrophysique* **31**, 475 (1968).
133. Fabian, A. C., Pringle, J. E. & Rees, M. J. Tidal capture formation of binary systems and X-ray sources in globular clusters. *Mon. Not. R. Astron. Soc.* **172**, 15p–18p (1975).
134. Lee, H. M. & Ostriker, J. P. Cross sections for tidal capture binary formation and stellar merger. *Astrophys. J.* **310**, 176–188 (1986).

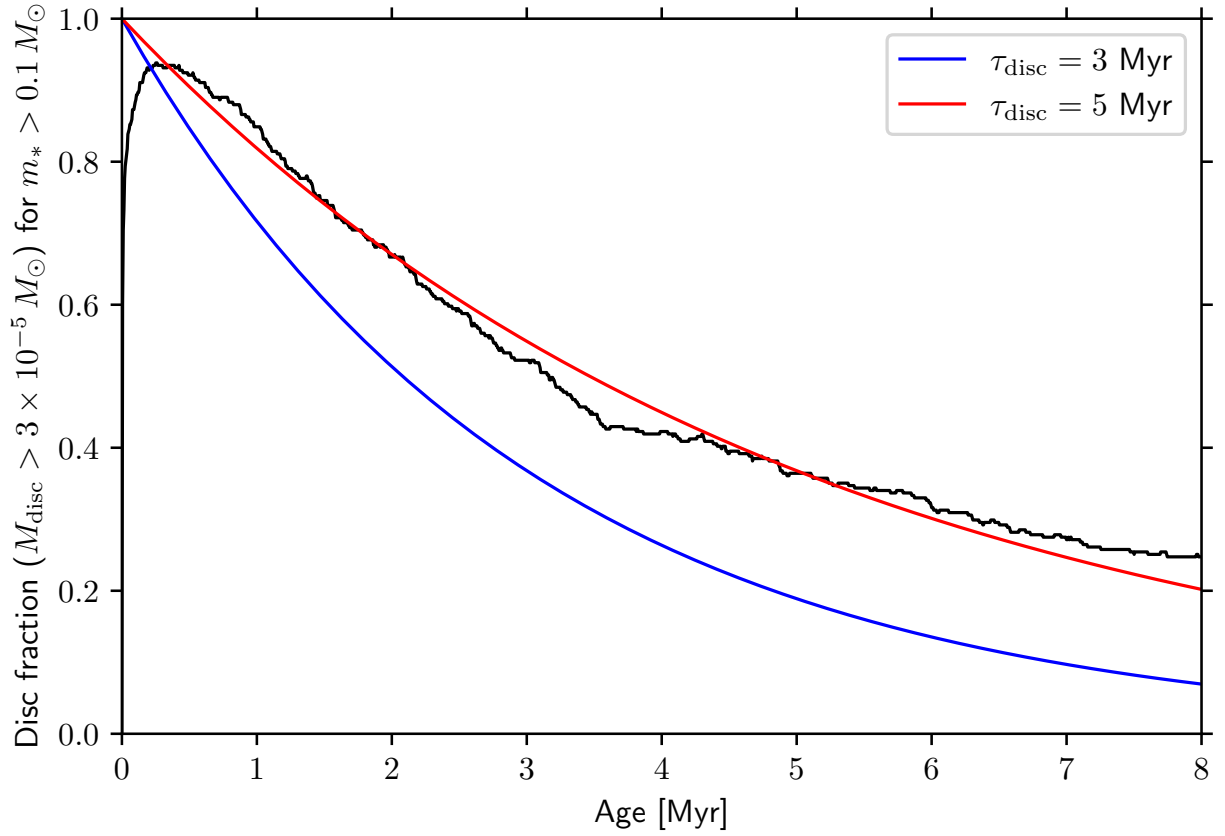
135. Dullemond, C. P., Kimmig, C. N. & Zanazzi, J. J. On the equations of warped disc dynamics. *Mon. Not. R. Astron. Soc.* **511**, 2925–2947 (2022).
136. Marino, S., Perez, S. & Casassus, S. Shadows Cast by a Warp in the HD 142527 Protoplanetary Disk. *Astrophys. J. Let.* **798**, L44 (2015).
137. Hartmann, L. & Kenyon, S. J. The FU Orionis Phenomenon. *Annu. Rev. Astron. Astrophys.* **34**, 207–240 (1996).
138. Herbig, G. H. On the interpretation of FU orionis. *Vistas in Astronomy* **8**, 109–125 (1966).
139. Herbig, G. H. Eruptive phenomena in early stellar evolution. *Astrophys. J.* **217**, 693–715 (1977).
140. Bonnell, I. & Bastien, P. A Binary Origin for FU Orionis Stars. *Astrophys. J. Let.* **401**, L31 (1992).
141. Borchert, E. M. A., Price, D. J., Pinte, C. & Cuello, N. On the rise times in FU Orionis events. *Mon. Not. R. Astron. Soc.* **510**, L37–L41 (2022).
142. Lin, D. N. C., Papaloizou, J. & Faulkner, J. On the evolution of accretion disc flow in cataclysmic variables - III. Outburst properties of constant and uniform α model discs. *Mon. Not. R. Astron. Soc.* **212**, 105–149 (1985).
143. Clarke, C. J. & Syer, D. Low-mass companions to T Tauri stars: a mechanism for rapid-rise FU Orionis outbursts. *Mon. Not. R. Astron. Soc.* **278**, L23–L27 (1996).

144. Lodato, G. & Clarke, C. J. Massive planets in FU Orionis discs: implications for thermal instability models. *Mon. Not. R. Astron. Soc.* **353**, 841–852 (2004).
145. Zurlo, A. *et al.* The environment around young eruptive stars. SPHERE/IRDIS polarimetric imaging of 7 protostars. *arXiv e-prints* arXiv:2403.12124 (2024).
146. Hales, A. S. *et al.* Discovery of an Accretion Streamer and a Slow Wide-angle Outflow around FU Orionis. *Astrophys. J.* **966**, 96 (2024).
147. Grant, S. L. *et al.* The $\dot{M} - M_{\text{disk}}$ Relationship for Herbig Ae/Be Stars: A Lifetime Problem for Disks with Low Masses? *Astron. J.* **166**, 147 (2023).
148. Silverberg, S. M. *et al.* Peter pan disks: Long-lived accretion disks around young m stars. *The Astrophysical Journal* **890**, 106 (2020). URL <https://dx.doi.org/10.3847/1538-4357/ab68e6>.
149. Lee, J., Song, I. & Murphy, S. 2MASS J15460752-6258042: a mid-M dwarf hosting a prolonged accretion disc. *Mon. Not. R. Astron. Soc.* **494**, 62–68 (2020).
150. Ansdell, M. *et al.* An ALMA Survey of λ Orionis Disks: From Supernovae to Planet Formation. *Astron. J.* **160**, 248 (2020).
151. Hamer, J. H. & Schlaufman, K. C. Hot Jupiters Are Destroyed by Tides While Their Host Stars Are on the Main Sequence. *Astron. J.* **158**, 190 (2019).
152. Winter, A. J., Kruijssen, J. M. D., Longmore, S. N. & Chevance, M. Stellar clustering shapes the architecture of planetary systems. *Nature* **586**, 528–532 (2020).

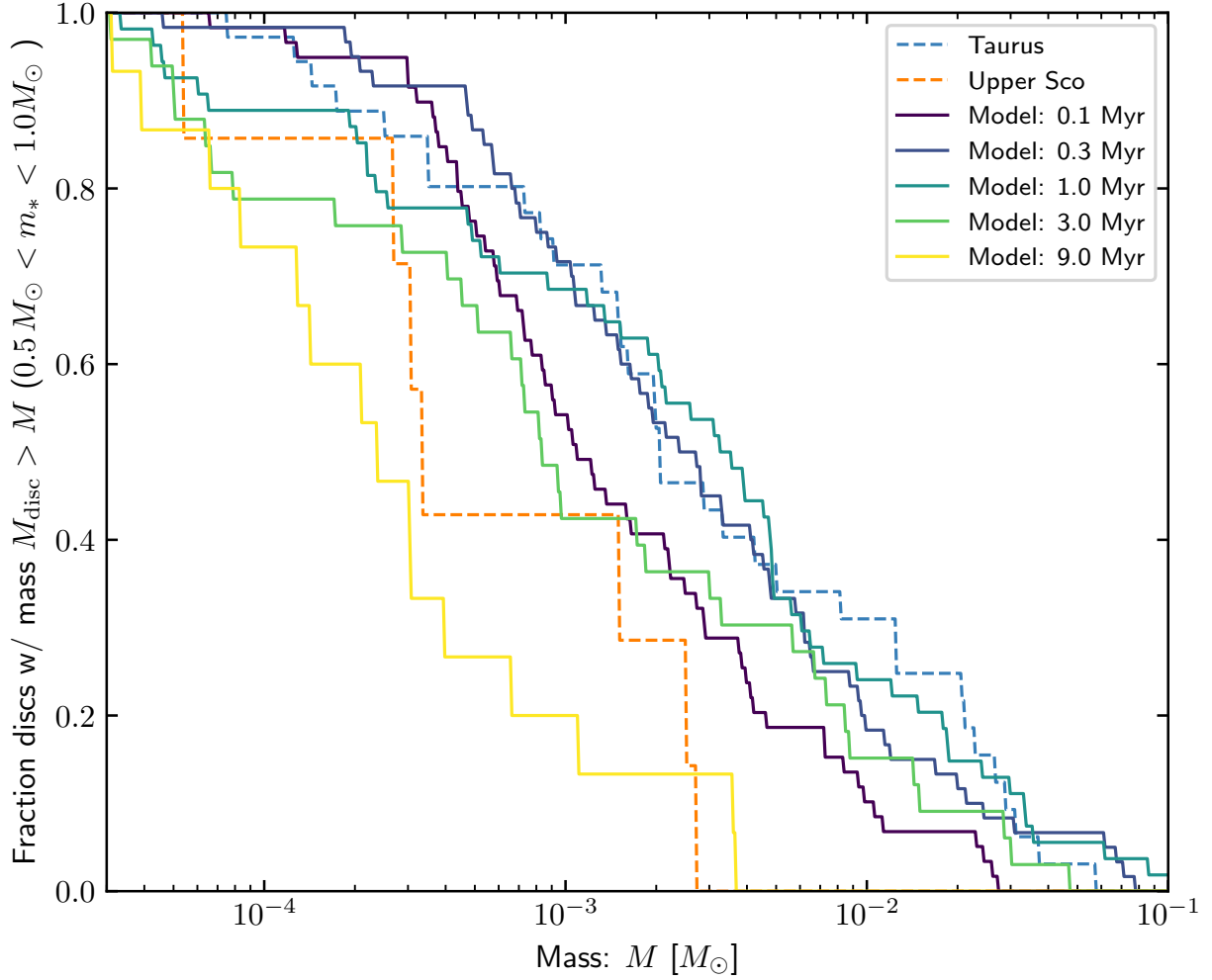
153. Miyazaki, S. & Masuda, K. Evidence That the Occurrence Rate of Hot Jupiters around Sun-like Stars Decreases with Stellar Age. *Astron. J.* **166**, 209 (2023).
154. Longmore, S. N., Chevance, M. & Kruijssen, J. M. D. The Impact of Stellar Clustering on the Observed Multiplicity and Orbital Periods of Planetary Systems. *Astrophys. J. Let.* **911**, L16 (2021).
155. Winter, A. J. & Alexander, R. An upper limit for the growth of inner planets? *Mon. Not. R. Astron. Soc.* **505**, 869–888 (2021).
156. Zink, J. K. *et al.* Scaling K2. VI. Reduced Small-planet Occurrence in High-galactic-amplitude Stars. *Astron. J.* **165**, 262 (2023).



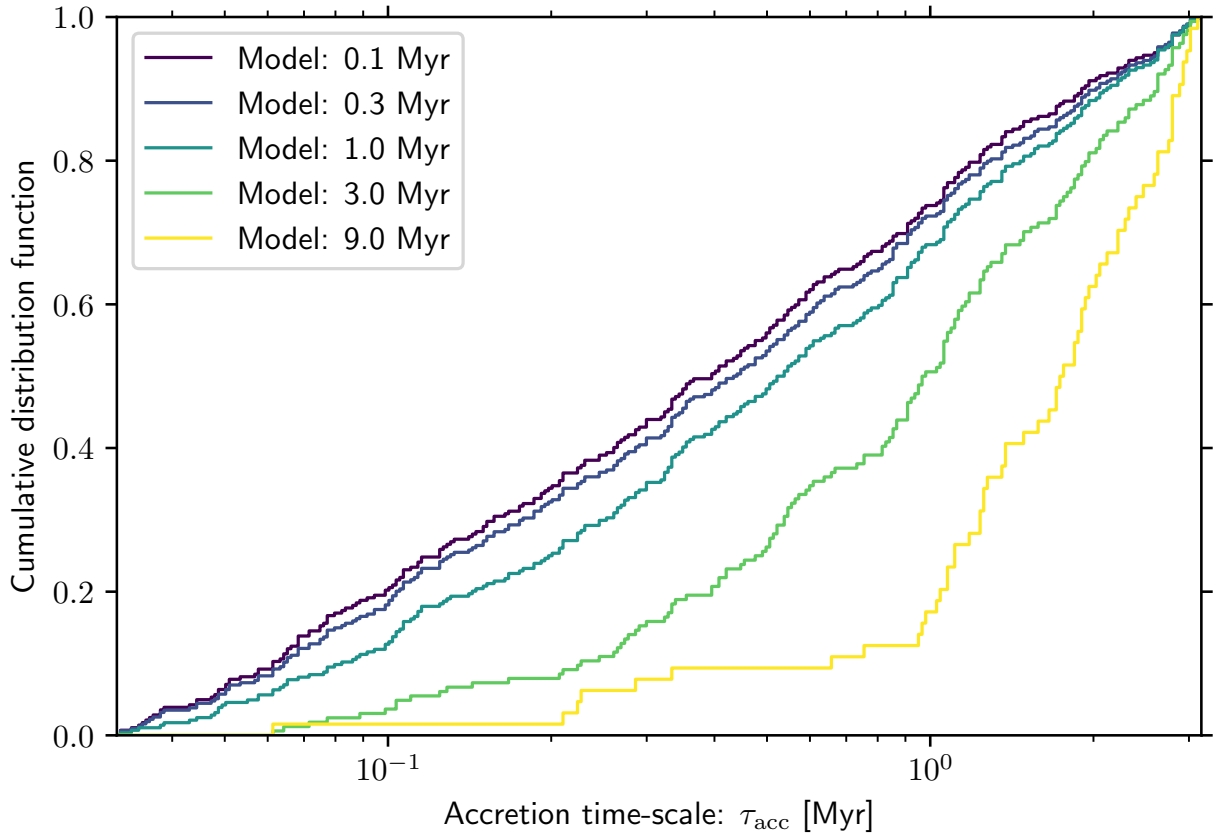
Extended Data Figure 1 — Mass distribution function of local star forming regions. Number of regions obtained by drawing 10^5 samples from the mass function via the excursion set formalism for GMCs (blue points) based on random sampling of Fourier space for ISM turbulence in the solar neighbourhood. We have normalised the y -axis such that we show the average number of regions younger than 10 Myr that are expected to be found within 200 pc. We highlight in yellow the region which is well-sampled, corresponding to typical local star forming regions which are surveyed for protoplanetary disc properties. In cyan, we show the range of initial GMC masses we consider to generate our disc population synthesis. In orange, we show the same mass function assuming a fixed star formation efficiency $\epsilon = 0.5$.



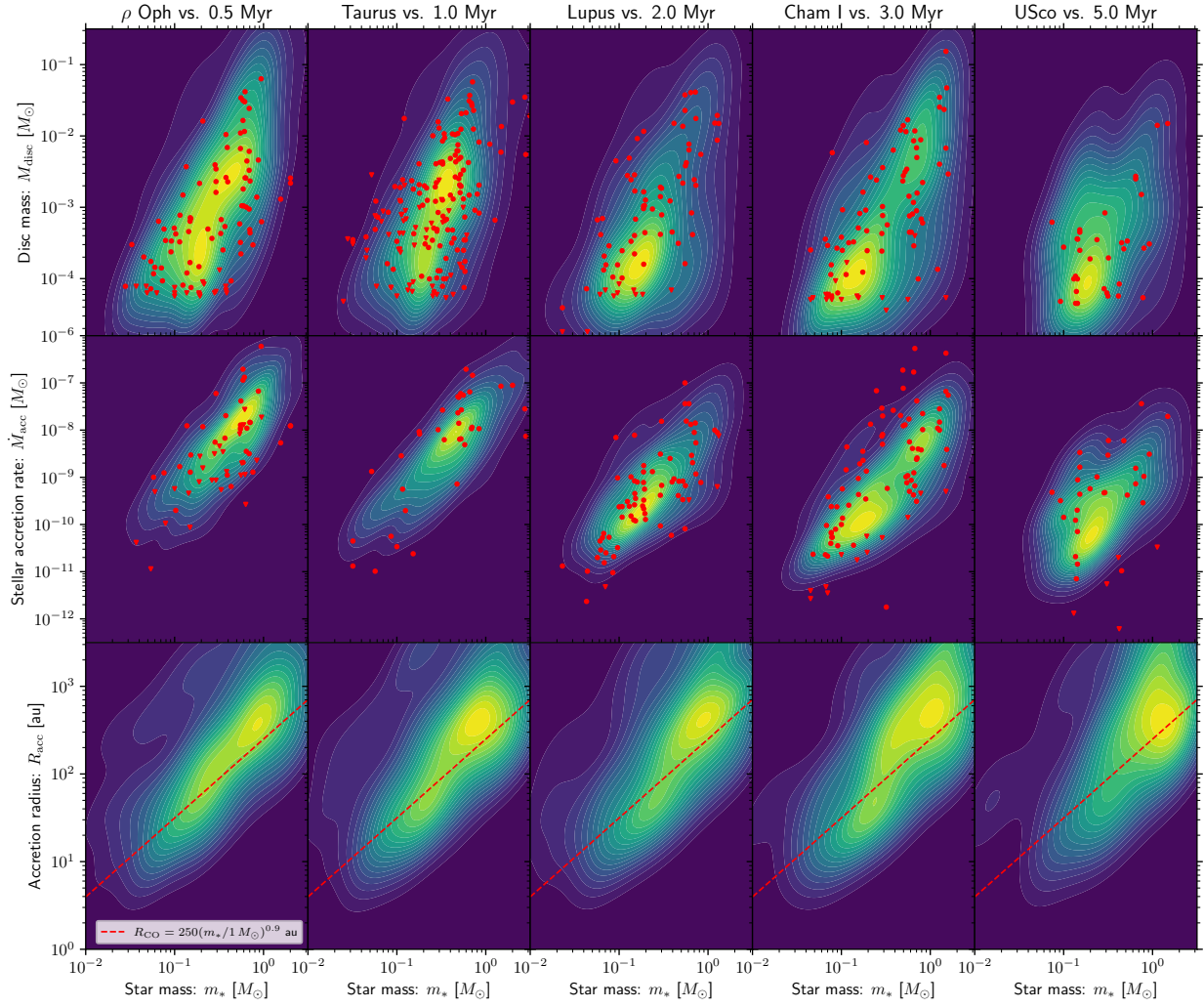
Extended Data Figure 2 — Disc survival fraction over time. Fraction of surviving discs in our model (black line), defined to be discs which have a mass $M_{\text{disc}} > 3 \times 10^{-5} M_{\odot}$ for stars with masses in the range $0.1-3 M_{\odot}$. We show the evolution of disc fraction given by $\exp(-t/\tau_{\text{disc}})$ for $\tau_{\text{disc}} = 3 \text{ Myr}$ ¹ and 5 Myr ¹⁰⁵ as blue and red lines respectively.



Extended Data Figure 3 — Disc mass distribution evolution. Cumulative distribution of disc masses at different times in our model (solid lines) compared to the observed distribution (dashed lines) for Taurus (blue) and Upper Sco (orange). We include only two observed disc populations for clarity. Shaded region represents the statistical uncertainty interval for observational datasets.

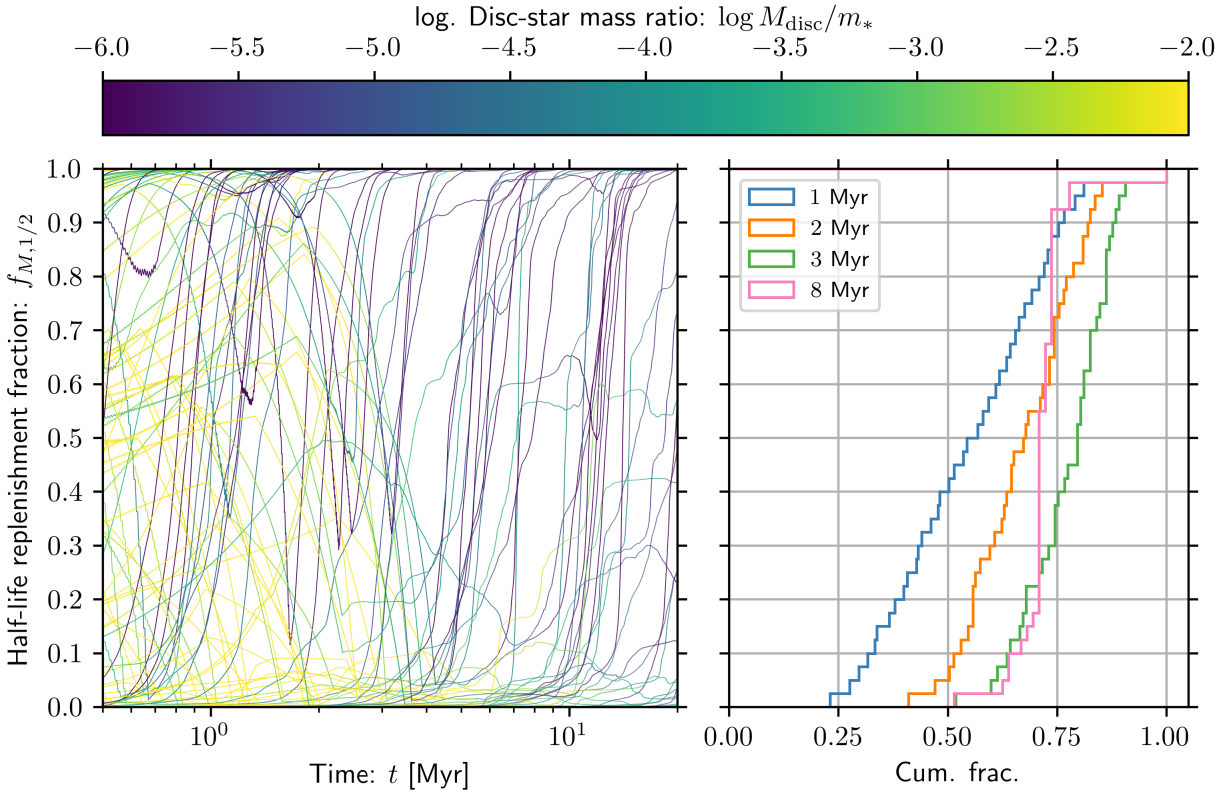


Extended Data Figure 4 — Evolution of the accretion time-scale distribution. Cumulative distribution of the accretion time-scales τ_{acc} at different times for surviving discs in our model. This evolution is purely due to discs with short accretion time-scales dropping out of the sample.

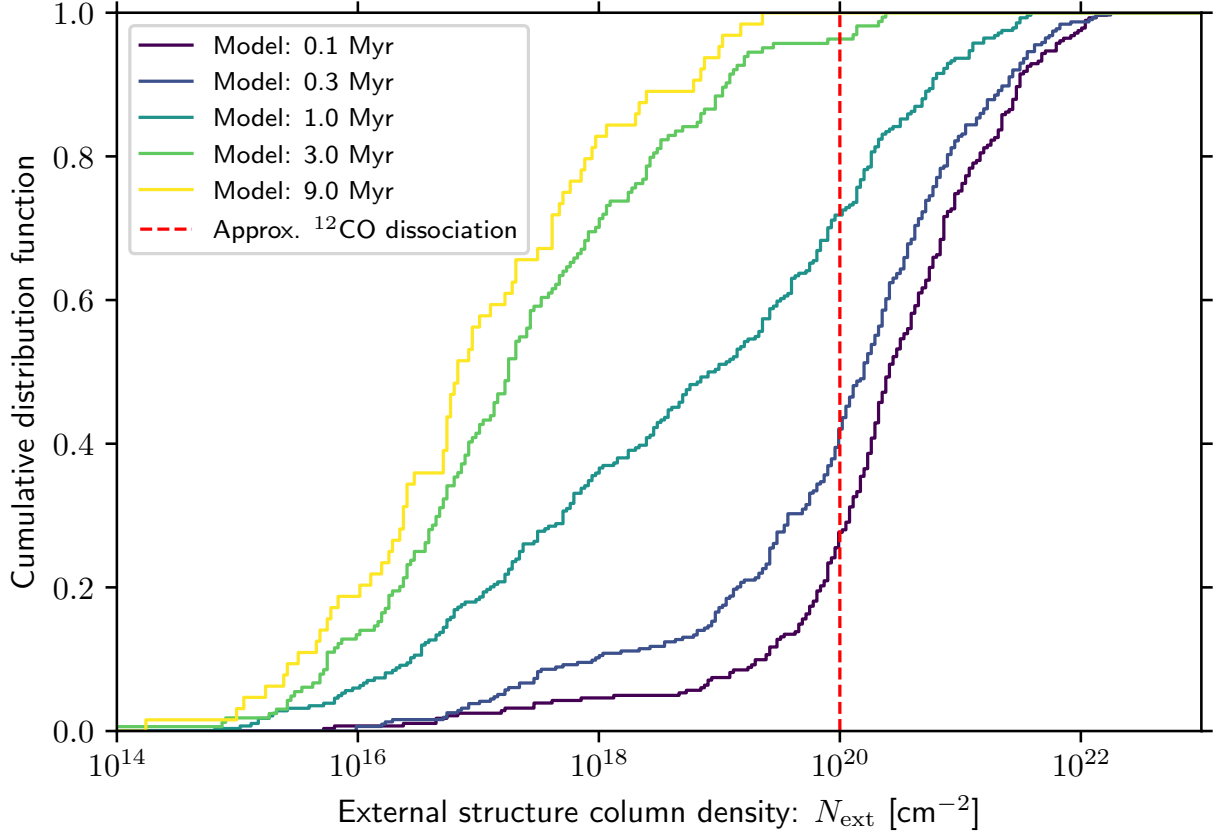


Extended Data Figure 5 — Disc properties for a model with non-negligible initial disc mass. As in

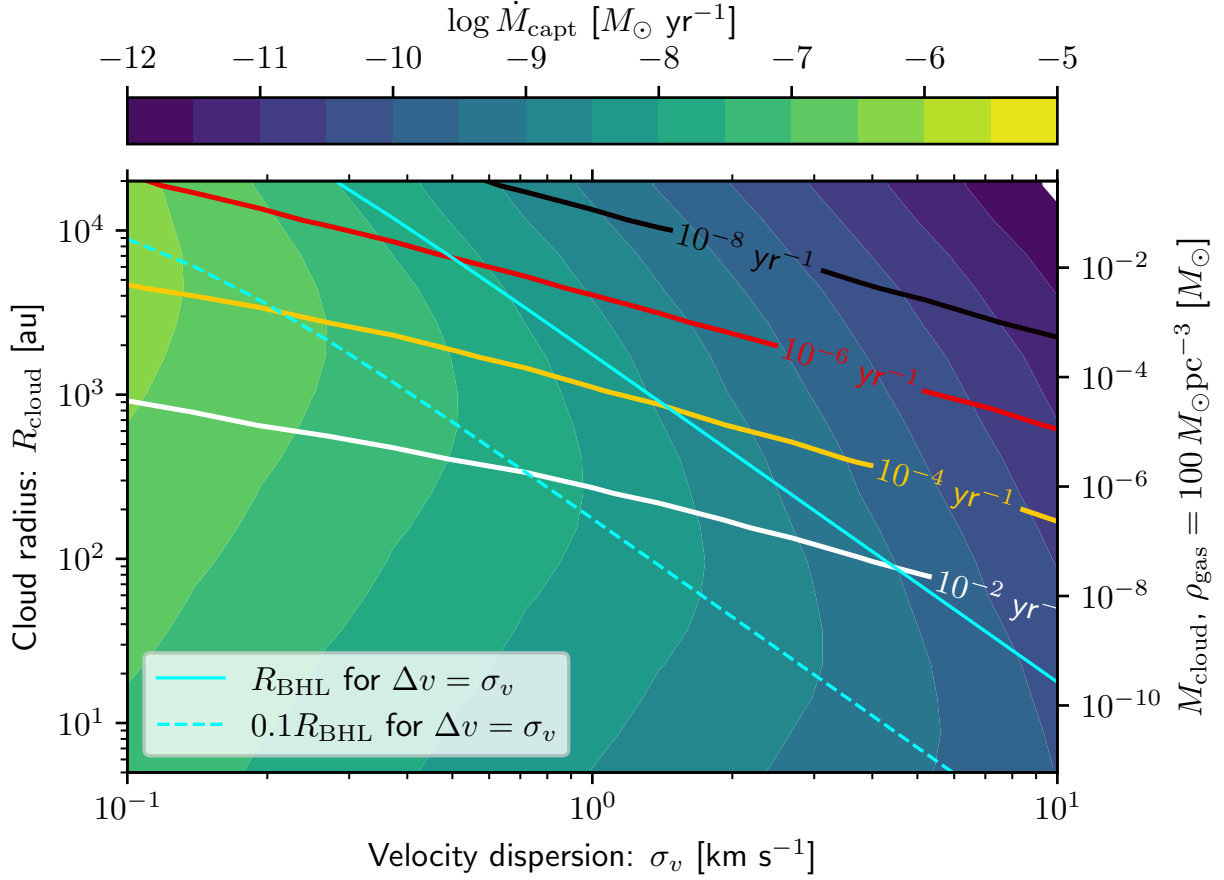
Figure 2, but for an initial disc mass $M_{\text{disc}}(t = 0) = 0.01(m_*/1 M_{\odot})^2 M_{\odot}$ with 1 dex of scatter.



Extended Data Figure 6 — Half-life replenishment fractions for a model with non-negligible initial disc mass. As in Figure 3, but for an initial disc mass $M_{\text{disc}}(t = 0) = 0.01(m_*/1 M_\odot)^2 M_\odot$ with 1 dex of scatter.



Extended Data Figure 7 — Approximate column density of external structure from our model. The column number density of material assuming a mean molecular mass $\mu = 2.3$ and $\epsilon_{\text{geo}} = 1$ following equation 23 for the surviving discs in our fiducial model. The colours of the lines represent the age of the discs. The red vertical dashed line represents an approximate column density for photodissociation of ^{12}CO , based on a self-shielding column of 10^{15} cm^{-2} and abundance relative to hydrogen of 10^{-5} .¹⁰⁴



Extended Data Figure 8 — Accretion rate from the ISM due to tidal cloud capture. The expected mass accretion rate \dot{M}_{capt} onto a disc around a star of mass $m_* = 1 M_{\odot}$ due to gravitationally focused cloudlet capture in a gaseous medium of density $\rho = 100 M_{\odot} \text{pc}^{-3} = 6.77 \times 10^{-21} \text{g cm}^{-3}$. The colour bar shows the averaged mass accretion rate, and the rate Γ_{capt} of individual cloudlet capture is shown by contours. The BHL radius is shown as a solid cyan line, while the optimum clouds contributing to mass accretion have $R_{\text{cloud}} \approx 0.1 R_{\text{BHL}}$ (dashed cyan line).